

ELIMINATING OVERSATURATION AND ARTIFACTS OF HIGH GUIDANCE SCALES IN DIFFUSION MODELS

Anonymous authors

Paper under double-blind review

ABSTRACT

Classifier-free guidance (CFG) is crucial for improving both generation quality and alignment between the input condition and final output in diffusion models. While a high guidance scale is generally required to enhance these aspects, it also causes oversaturation and unrealistic artifacts. In this paper, we revisit the CFG update rule and introduce modifications to address this issue. We first decompose the update term in CFG into parallel and orthogonal components with respect to the conditional model prediction and observe that the parallel component primarily causes oversaturation, while the orthogonal component enhances image quality. Accordingly, we propose down-weighting the parallel component to achieve high-quality generations without oversaturation. Additionally, we draw a connection between CFG and gradient ascent and introduce a new rescaling and momentum method for the CFG update rule based on this insight. Our approach, termed adaptive projected guidance (APG), retains the quality-boosting advantages of CFG while enabling the use of higher guidance scales without oversaturation. APG is easy to implement and introduces practically no additional computational overhead to the sampling process. Through extensive experiments, we demonstrate that APG is compatible with various conditional diffusion models and samplers, leading to improved FID, recall, and saturation scores while maintaining precision comparable to CFG, making our method a superior plug-and-play alternative to standard classifier-free guidance.¹



Figure 1: Classifier-free guidance is essential for generating high-quality images but causes oversaturation and unrealistic artifacts in the outputs. We introduce APG, a novel method that keeps the quality of CFG but significantly reduces its harmful oversaturation. Both images are generated with Stable Diffusion XL (Podell et al., 2023) and a guidance scale of 15.

¹All visual results in the paper are best viewed in color and when zoomed in.

1 INTRODUCTION

Diffusion models (Sohl-Dickstein et al., 2015; Ho et al., 2020; Song et al., 2021b) are a class of generative models that learn the data distribution by reversing a forward process that adds noise to the data until the samples are indistinguishable from pure noise. Although the theory suggests that simulating the backward process in diffusion models should result in correct sampling from the data distribution, unguided sampling from diffusion models often results in low-quality images that do not align well with the input condition. Accordingly, classifier-free guidance (Ho & Salimans, 2022) has been established as an essential tool in modern diffusion models for increasing the quality of generations and the alignment between the condition and the generated image, albeit at the cost of reduced diversity (Ho & Salimans, 2022; Sadat et al., 2024a).

Modern text-to-image models, such as Stable Diffusion (Rombach et al., 2022), generally require high guidance scales in order for the generations to have better quality and align well with the input prompt. However, high guidance scales often result in oversaturated colors and simplified image compositions (Saharia et al., 2022b; Kynkäänniemi et al., 2024). Despite these disadvantages, high CFG scales are still used in practice due to their superior image quality compared to alternatives.

In this paper, we analyze the update rule of CFG and show that with a few modifications to how the CFG update is applied at inference, we can vastly mitigate the oversaturation and artifacts of high guidance scales. First, we show that the CFG update rule can be decomposed into two components, one that is parallel to the conditional model prediction, and one that is orthogonal to this prediction. We show that the orthogonal element is mainly responsible for improving image quality, while the parallel part primarily adds contrast and saturation to the output. To the best of our knowledge, this is the first study that disentangles these two effects in CFG.

Additionally, we establish a connection between the CFG update rule and stochastic gradient ascent. This insight leads us to explore a rescaled version of the CFG update direction and incorporate a momentum term, similar to adaptive optimization methods. The rescaling is motivated by the need to control large update norms, which can cause significant drifts in the sampling process. To prevent this, we constrain the updates to lie within a sphere. For the momentum term, unlike with traditional optimization, we apply a *negative* value to introduce a repulsive effect between consecutive updates, effectively down-weighting components already present in previous steps. We refer to this as *reverse momentum*. By combining rescaling, reverse momentum, and projection, we introduce a new method, called adaptive projected guidance (APG), which allows the use of higher guidance scales without oversaturation or degradation in image quality.

Through extensive experiments with several diffusion models, such as EDM2 (Karras et al., 2023) and Stable Diffusion (Rombach et al., 2022), we demonstrate that APG can utilize high guidance scales without encountering oversaturation. As a result, we conclude that APG significantly expands the usable guidance range in practice and mitigates the harmful effects of CFG at high guidance scales. Our quantitative analysis shows that replacing CFG with APG improves FID, recall, and saturation scores while maintaining precision similar to CFG. Furthermore, when combined with Stable Diffusion 3 (Esser et al., 2024), APG enhances the consistency of text rendering in generated images. We also demonstrate that APG is compatible with distilled models that use fewer sampling steps, such as SDXL-Lightning (Lin et al., 2024b). A representative visual comparison between CFG and APG is shown in Figure 1.

2 RELATED WORK

Score-based diffusion models (Song & Ermon, 2019; Song et al., 2021b; Sohl-Dickstein et al., 2015; Ho et al., 2020) learn data distributions by reversing a forward diffusion process that gradually corrupts data into Gaussian noise. These models have rapidly outperformed previous generative modeling methods in terms of fidelity and diversity (Nichol & Dhariwal, 2021; Dhariwal & Nichol, 2021), setting new benchmarks across various domains. They have achieved state-of-the-art results in unconditional image generation (Dhariwal & Nichol, 2021; Karras et al., 2022), text-to-image generation (Ramesh et al., 2022; Saharia et al., 2022b; Balaji et al., 2022; Rombach et al., 2022; Podell et al., 2023; Yu et al., 2022), video generation (Blattmann et al., 2023b;a; Gupta et al., 2023), image-to-image translation (Saharia et al., 2022a; Liu et al., 2023a), and audio generation (Chen et al., 2021; Kong et al., 2021; Huang et al., 2023).

Since the introduction of the DDPM model (Ho et al., 2020), numerous advancements have been made, such as improved network architectures (Hooeboom et al., 2023; Karras et al., 2023; Peebles & Xie, 2022; Dhariwal & Nichol, 2021), enhanced sampling algorithms (Song et al., 2021a; Karras et al., 2022; Liu et al., 2022b; Lu et al., 2022a; Salimans & Ho, 2022), and new training techniques (Nichol & Dhariwal, 2021; Karras et al., 2022; Song et al., 2021b; Salimans & Ho, 2022; Rombach et al., 2022). Despite these advancements, diffusion guidance, including both classifier and classifier-free guidance (Dhariwal & Nichol, 2021; Ho & Salimans, 2022), remains crucial in enhancing generation quality and improving alignment between the condition and the output image (Nichol et al., 2022), albeit at the cost of reduced diversity and oversaturated outputs.

A recent line of work, such as CADs (Sadat et al., 2024a) and interval guidance (IG) (Kynkäänniemi et al., 2024), has focused on enhancing the diversity of generations at higher guidance scales. In contrast, our proposed method, APG, specifically addresses the oversaturation issue in CFG, as these diversity-boosting methods still struggle with oversaturation at higher guidance scales. In Appendix C.1, we demonstrate that APG can be combined with CADs and IG to achieve diverse generations without encountering oversaturation problems.

Dynamic thresholding (Saharia et al., 2022b) was introduced to mitigate the saturation effect in CFG, but it is not directly applicable to latent diffusion models (since it assumes pixel values are between $[-1, 1]$) and tends to produce images lacking in detail. Another approach, CFG Rescale (Lin et al., 2024a), aims to reduce overexposure in generated images by rescaling the standard deviation of the predictions after applying CFG. However, we demonstrate that our method is noticeably more effective at reducing oversaturation compared to CFG Rescale.

Orthogonal projection has been explored in the context of text-to-3D generation (Armandpour et al., 2023) and non-linear guidance (Zheng & Lan, 2024), but none of these methods tackle the saturation issue at higher guidance scales. We also demonstrate that naive projection has minimal impact on CFG behavior, as it must be applied to the denoised predictions to be effective. Additionally, we incorporate rescaling and reverse momentum to further mitigate the adverse effects of CFG at higher guidance scales. We show that APG can be applied to various conditional diffusion models while adding practically no overhead to the sampling process.

3 BACKGROUND

We provide a brief overview of diffusion models in this section. Let $\mathbf{x} \sim p_{\text{data}}(\mathbf{x})$ represent a data point, and let $\mathbf{z}_t = \mathbf{x} + \sigma(t)\epsilon$ describe a forward process of the diffusion model that introduces noise to the data, where $t \in [0, 1]$ is the time step. Here, $\sigma(t)$ is the noise schedule, which determines the amount of information destroyed at each time step t , with $\sigma(0) = 0$ and $\sigma(1) = \sigma_{\text{max}}$. Karras et al. (2022) demonstrated that this forward process is equivalent to the following ordinary differential equation (ODE):

$$d\mathbf{z}_t = -\dot{\sigma}(t)\sigma(t) \nabla_{\mathbf{z}_t} \log p_t(\mathbf{z}_t) dt, \quad (1)$$

where $p_t(\mathbf{z}_t)$ denotes the time-dependent distribution of noisy samples, with $p_0 = p_{\text{data}}$ and $p_1 = \mathcal{N}(\mathbf{0}, \sigma_{\text{max}}^2 \mathbf{I})$. With access to the time-dependent score function $\nabla_{\mathbf{z}_t} \log p_t(\mathbf{z}_t)$, one can sample from the data distribution p_{data} by solving the ODE backward in time (from $t = 1$ to $t = 0$). The unknown score function $\nabla_{\mathbf{z}_t} \log p_t(\mathbf{z}_t)$ is estimated using a neural denoiser $D_{\theta}(\mathbf{z}_t, t)$, which is trained to predict the clean samples \mathbf{x} from the corresponding noisy samples \mathbf{z}_t . This framework also allows for conditional generation by training a denoiser $D_{\theta}(\mathbf{z}_t, t, \mathbf{y})$ that incorporates additional input signals \mathbf{y} , such as class labels or text prompts.

Classifier-free guidance (CFG) CFG is an inference method designed to enhance the quality of generated outputs by combining the predictions of a conditional model and an unconditional model (Ho & Salimans, 2022). Given a null condition $\mathbf{y}_{\text{null}} = \emptyset$ for the unconditional case, CFG modifies the denoiser’s output at each sampling step as follows:

$$\hat{D}_{\text{CFG}}(\mathbf{z}_t, t, \mathbf{y}) = D_{\theta}(\mathbf{z}_t, t, \mathbf{y}_{\text{null}}) + w(D_{\theta}(\mathbf{z}_t, t, \mathbf{y}) - D_{\theta}(\mathbf{z}_t, t, \mathbf{y}_{\text{null}})), \quad (2)$$

where $w = 1$ represents the non-guided case. The unconditional model $D_{\theta}(\mathbf{z}_t, t, \mathbf{y}_{\text{null}})$ is trained by randomly applying the null condition $\mathbf{y}_{\text{null}} = \emptyset$ to the denoiser’s input for a portion of training. Alternatively, a separate denoiser can be trained to estimate the unconditional score in Equation (2) (Karras et al., 2023). Similar to the truncation method used in GANs (Brock et al., 2019), CFG improves the quality of images but reduces diversity (Murphy, 2023).

4 ADAPTIVE PROJECTED GUIDANCE

We now present our method for addressing oversaturation and artifacts in CFG at high guidance scales. Let $\Delta D_t = D_\theta(\mathbf{z}_t, t, \mathbf{y}) - D_\theta(\mathbf{z}_t, t, \mathbf{y}_{\text{null}})$ be the CFG update direction at time step t . Note that Equation (2) can now be written as

$$\hat{D}_{\text{CFG}}(\mathbf{z}_t, t, \mathbf{y}) = D_\theta(\mathbf{z}_t, t, \mathbf{y}) + (w - 1)\Delta D_t. \quad (3)$$

(See Appendix A for the derivation.) We use Equation (3) for the rest of this paper to motivate our changes. APG has three elements: (1) projection, (2) rescaling, and (3) reverse momentum. We discuss each component below.

Orthogonal projection First, note that we can decompose ΔD_t into two different components: ΔD_t^\parallel , which is parallel to $D_\theta(\mathbf{z}_t, t, \mathbf{y})$, and ΔD_t^\perp , which is orthogonal to $D_\theta(\mathbf{z}_t, t, \mathbf{y})$, i.e., $\Delta D_t = \Delta D_t^\perp + \Delta D_t^\parallel$. We can compute ΔD_t^\parallel via orthogonal projection, with

$$\Delta D_t^\parallel = \frac{\langle \Delta D_t, D_\theta(\mathbf{z}_t, t, \mathbf{y}) \rangle}{\langle D_\theta(\mathbf{z}_t, t, \mathbf{y}), D_\theta(\mathbf{z}_t, t, \mathbf{y}) \rangle} D_\theta(\mathbf{z}_t, t, \mathbf{y}). \quad (4)$$

We then have $\Delta D_t^\perp = \Delta D_t - \Delta D_t^\parallel$. We observe that the orthogonal component is chiefly responsible for improvements in image quality, while the parallel component increases saturation in the generations as shown in Figure 2.

Accordingly, we modify the update direction to form $\Delta D_t(\eta) = \Delta D_t^\perp + \eta \Delta D_t^\parallel$, where $\eta \leq 1$ is a hyperparameter. Note that $\Delta D_t(1)$ is identical to the unmodified CFG update direction described above. We show that reducing the strength of the parallel component (i.e. setting η close to zero) significantly reduces saturation and results in more realistic generations at higher guidance scales.

The intuition behind the saturating effect of the parallel component is helped by thinking of the output $D_\theta(\mathbf{z}_t, t, \mathbf{y})$ as an image with a typical range of values.² When an update parallel to this image is added, it serves to create a ‘‘gain,’’ pushing the values toward the extremes of their range. This gain effect can be seen by direct calculation:

$$D_\theta(\mathbf{z}_t, t, \mathbf{y}) + (w - 1)\Delta D_t^\parallel = \left[1 + (w - 1) \frac{\|\Delta D_t^\parallel\|}{\|D_\theta(\mathbf{z}_t, t, \mathbf{y})\|} \right] D_\theta(\mathbf{z}_t, t, \mathbf{y}), \quad (5)$$

where we note that the term in brackets on the right-hand side is greater than one for $w > 1$. Thus, this term only adds saturation to the predictions $D_\theta(\mathbf{z}_t, t, \mathbf{y})$ during each inference step, much like multiplying pixel values by a number greater than one. We show in Section 5.2 that reducing η and leaning more heavily on the orthogonal component significantly attenuates this saturation side effect in generations while maintaining the quality-boosting benefits of CFG.

Adding rescaling Next, we argue that the CFG update rule in Equation (3) can be interpreted as one step of gradient ascent on the ℓ_2 distance between the conditional and unconditional prediction, i.e., one step of gradient ascent on $\frac{1}{2} \|D_\theta(\mathbf{z}_t, t, \mathbf{y}) - D_\theta(\mathbf{z}_t, t, \mathbf{y}_{\text{null}})\|^2$ with a learning rate of $w - 1$. (See Appendix A for proof.) Inspired by this interpretation and normalized gradient ascent, we rescale the CFG update rule at each step to regulate the impact of each update. Specifically, we constrain ΔD_t to be inside a sphere with radius r via

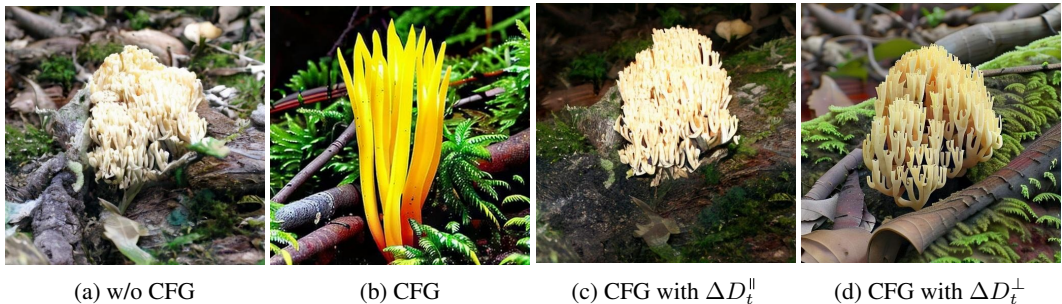
$$\Delta D_t \leftarrow \Delta D_t \cdot \min\left(1, \frac{r}{\|\Delta D_t\|}\right), \quad (6)$$

where r is a hyperparameter. This rescaling ensures that the CFG update ΔD_t stays closer to $D_\theta(\mathbf{z}_t, t, \mathbf{y})$, limiting drift at each sampling step if $\|\Delta D_t\|$ is large. As demonstrated in Section 5.2, this adjustment improves both FID and recall.

Adding reverse momentum Finally, leveraging the connection to gradient ascent, we introduce a reverse momentum term to the CFG update rule. We define the momentum for the CFG update direction as $\overline{\Delta D}_t \leftarrow \Delta D_t + \beta \overline{\Delta D}_t$, where $\overline{\Delta D}_t = 0$ initially. The momentum term accounts for the average values of past updates; however, unlike standard optimization methods, we use a *negative*

²This intuition also holds for the image-like representations in latent diffusion models.

216
217
218
219
220
221
222
223
224



225 Figure 2: Influence of the parallel and orthogonal components (ΔD_t^{\parallel} and ΔD_t^{\perp}) in CFG. (a) The
226 generation without CFG lacks quality and detail. (b) Applying CFG increases quality but introduces
227 oversaturation. (c) Applying CFG only with the parallel component ΔD_t^{\parallel} barely changes the output
228 quality compared to (a) and only increases saturation. (d) Applying CFG with only the orthogonal
229 part ΔD_t^{\perp} enhances image quality without causing oversaturation.

230
231
232
233
234
235
236
237
238
239
240
241
242



243 Figure 3: Illustrating the effect of APG on generated images . (a) Sampling without guidance leads to
244 low-quality generations. (b) CFG improves image quality but causes oversaturation. (c) Using APG
245 instead of CFG results in high-quality generations without oversaturation.

246
247
248
249
250
251
252
253
254
255

momentum strength $\beta < 0$. Intuitively, this pushes the model away from previous CFG update directions and encourages the model to focus more on the current update direction. As shown in Section 5.2, incorporating reverse momentum further enhances image quality (i.e., lower FID scores).

APG is easy to implement, and we provide the source code in Algorithm 1 (appendix). As shown in Section 5.2, it is crucial to convert the diffusion model’s outputs (e.g., predicted noise) into the denoised prediction $D_{\theta}(z_t, t, y)$ in order to perform the projection. Further details on obtaining $D_{\theta}(z_t, t, y)$ for common prediction types are discussed in Appendix B. Figure 3 demonstrates that using APG instead of CFG produces high-quality generations without oversaturation or the undesirable artifacts associated with high guidance scales.

256
257

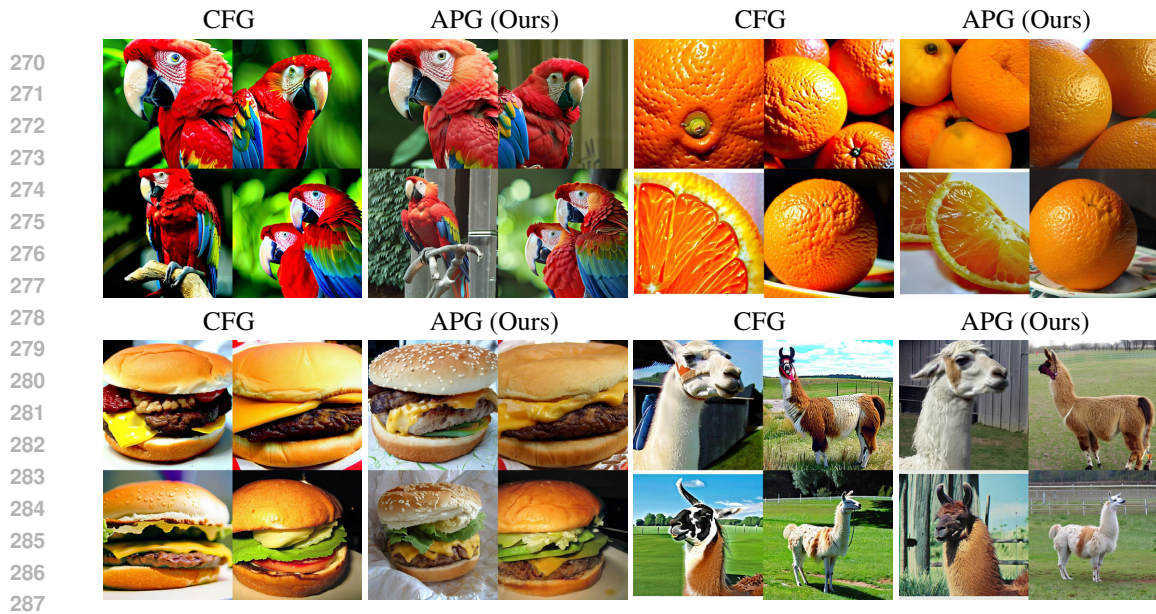
5 EXPERIMENTS AND RESULTS

258
259
260
261
262
263
264

Setup We mainly experiment with text-to-image generation with Stable Diffusion (Rombach et al., 2022) and class-conditional ImageNet (Russakovsky et al., 2015) generation using EDM2 (Karras et al., 2023) and DiT-XL/2 (Peebles & Xie, 2022). For all experiments, we use the default diffusion sampler from each model (e.g., Euler scheduler for Stable Diffusion XL) along with pretrained checkpoints and corresponding codebases to ensure consistency in weights and the sampling process with the original frameworks.

265
266
267
268
269

Distribution metrics We use Fréchet Inception Distance (FID) (Heusel et al., 2017) as our primary metric for evaluating both the quality and diversity of generated images due to its alignment with human judgment. Since FID is sensitive to small implementation details, we ensure that all models are evaluated under the same setup. For completeness, we also report precision (Kynkäänniemi et al., 2019) as an additional quality metric and recall (Kynkäänniemi et al., 2019) as a diversity metric.



288 Figure 4: Class-conditional generation results using EDM2 with $w = 4$. APG significantly reduces
 289 saturation in the generations while keeping the high-quality global structure of each image.



310 Figure 5: Text-to-image generation results using Stable Diffusion XL with $w = 15$. APG produces
 311 more realistic images compared to the oversaturated outputs of CFG.

312 **Color metrics** While FID measures the overall quality of generated images, we introduce specific
 313 metrics to directly assess saturation and contrast. To measure saturation, we convert each image from
 314 RGB to HSV and compute the mean of the saturation channel. We define contrast (also known as
 315 RMS contrast) as the standard deviation of pixel values after converting the image to grayscale. The
 316 final metrics are derived by averaging the saturation and contrast values across all generated images.
 317

318 5.1 MAIN RESULTS

319

320

321 **Qualitative results** Figures 4 and 5 present our qualitative results comparing APG with CFG for
 322 EDM2 and Stable Diffusion XL. We observe that, compared to CFG, APG generates more realistic
 323 images with noticeably lower saturation. Furthermore, APG appears to produce fewer artifacts in the
 final outputs, as illustrated in Figure 6. Additional visual results can be found in Appendix E.



Figure 6: Examples of artifacts in the CFG outputs that can be solved by using APG. We see that for all images, APG outputs follow the prompt with a more globally consistent generation.

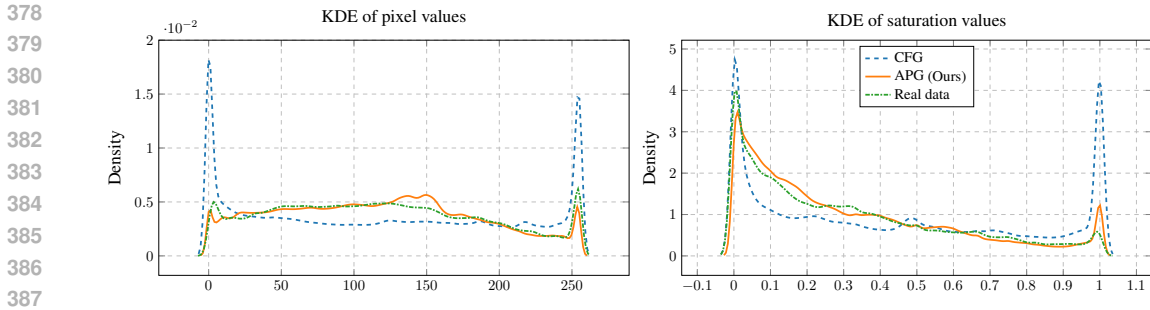
Table 1: Quantitative comparison between CFG and APG. APG consistently improves FID, recall and color metrics while maintaining similar or better precision compared to CFG.

Model	Guidance	FID ↓	Precision ↑	Recall ↑	Saturation ↓	Contrast ↓
EDM2-S ($w = 4$)	CFG	10.42	0.85	0.48	0.46	0.27
	APG (Ours)	6.49	0.85	0.62	0.33	0.21
EDM2-XXL ($w = 2$)	CFG	8.65	0.84	0.57	0.37	0.23
	APG (Ours)	4.94	0.83	0.67	0.31	0.21
DiT-XL/2 ($w = 4$)	CFG	19.14	0.92	0.35	0.37	0.25
	APG (Ours)	9.34	0.89	0.56	0.30	0.20
Stable Diffusion 2.1 ($w = 10$)	CFG	27.53	0.65	0.41	0.36	0.27
	APG (Ours)	22.21	0.67	0.49	0.27	0.22
Stable Diffusion XL ($w = 15$)	CFG	26.29	0.62	0.49	0.28	0.24
	APG (Ours)	25.35	0.64	0.50	0.18	0.17

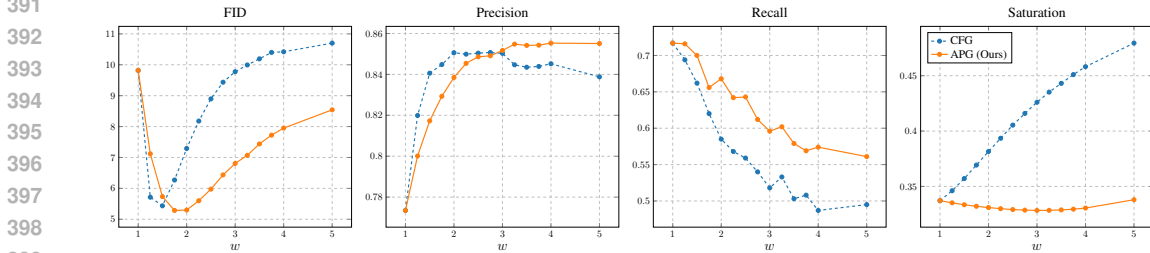
Quantitative results We next present a quantitative comparison between APG and CFG in Table 1. The table shows that APG outperforms CFG across multiple models, consistently achieving better FID and recall scores, as well as lower saturation and contrast. Moreover, APG demonstrates similar precision to CFG, indicating that the reduction in saturation does not compromise the quality of individual samples.

Distribution of pixel values Figure 7 presents the kernel density estimate (KDE) plot of RGB and saturation values for 100 images generated using CFG and APG, along with KDE plots for 100 real samples drawn from the evaluation subset of ImageNet. Compared to CFG, APG plots are more broadly distributed across the spectrum with less concentration at the extremes. This indicates that images generated with APG are closer to real data in terms of saturation and color composition.

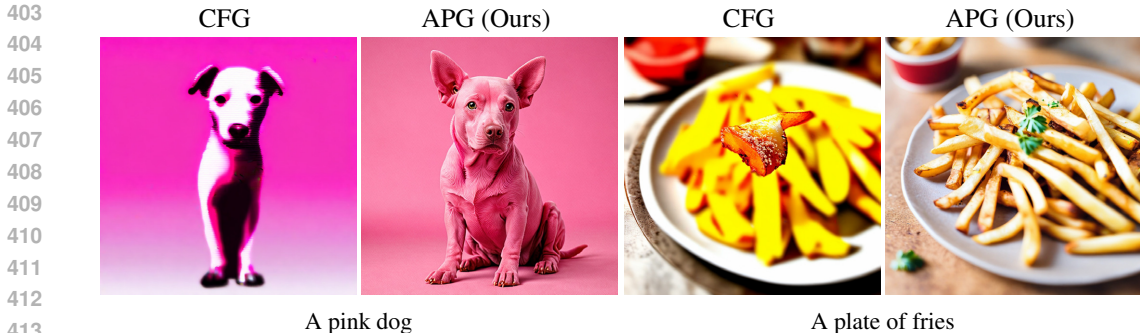
APG vs guidance scale In Figure 8, we demonstrate that as the guidance scale increases, APG consistently achieves lower FID and higher recall while maintaining similar or better precision compared to CFG. Additionally, CFG exhibits increasing saturation at higher guidance scales, whereas APG maintains a relatively constant saturation level. Therefore, APG allows the usage of higher guidance scales, achieving better FID and diversity without oversaturation.



378
379
380
381
382
383
384
385
386
387
388 Figure 7: Kernel density estimates of pixel and saturation values for two sets of samples generated
389 with CFG and APG. Compared to CFG, images generated with APG show less concentration around
390 saturated pixels, indicated by the spikes at the extreme values in both plots.



391
392
393
394
395
396
397
398
399
400 Figure 8: Comparison between CFG and APG as the guidance scale increases. APG offers better
401 FID and recall while maintaining similar or better precision to CFG at higher guidance scales.



402
403
404
405
406
407
408
409
410
411
412
413
414 Figure 9: Showcasing the compatibility of APG with distilled diffusion models using SDXL-
415 Lightning. Compared to CFG, using APG does not result in degradation in the output quality.

416
417
418 **Improving diversity** While APG is designed to address oversaturation at high guidance scales, we
419 also observed that it can enhance the diversity of generations. As shown in Table 1 and Figure 8, APG
420 improves distribution coverage (i.e., higher recall) while maintaining precision comparable to CFG.
421 Additional qualitative results illustrating the enhanced diversity are provided in Figure 17 (appendix).

422
423 **Using APG with distilled models** A common issue with CFG is that it degrades the quality of final
424 outputs when applied to distilled models with fewer sampling steps (e.g., 8-step SDXL-Lightning
425 (Lin et al., 2024c)). In this section, we show that APG does not encounter this problem and can
426 be effectively applied to distilled models. Figure 9 demonstrates that replacing CFG with APG
427 significantly improves generation quality. Extended results with additional models are provided in
428 Appendix C.3, along with more visual examples in Appendix E.

429
430 **Text spelling with Stable Diffusion 3** Next, we demonstrate that integrating APG with Stable
431 Diffusion 3 (Esser et al., 2024) enhances the consistency of text rendering in generated images. As
shown in Figure 10, APG produces more accurate spelling in the generated images compared to
standard CFG. More visual results are given in Figure 20 (appendix).

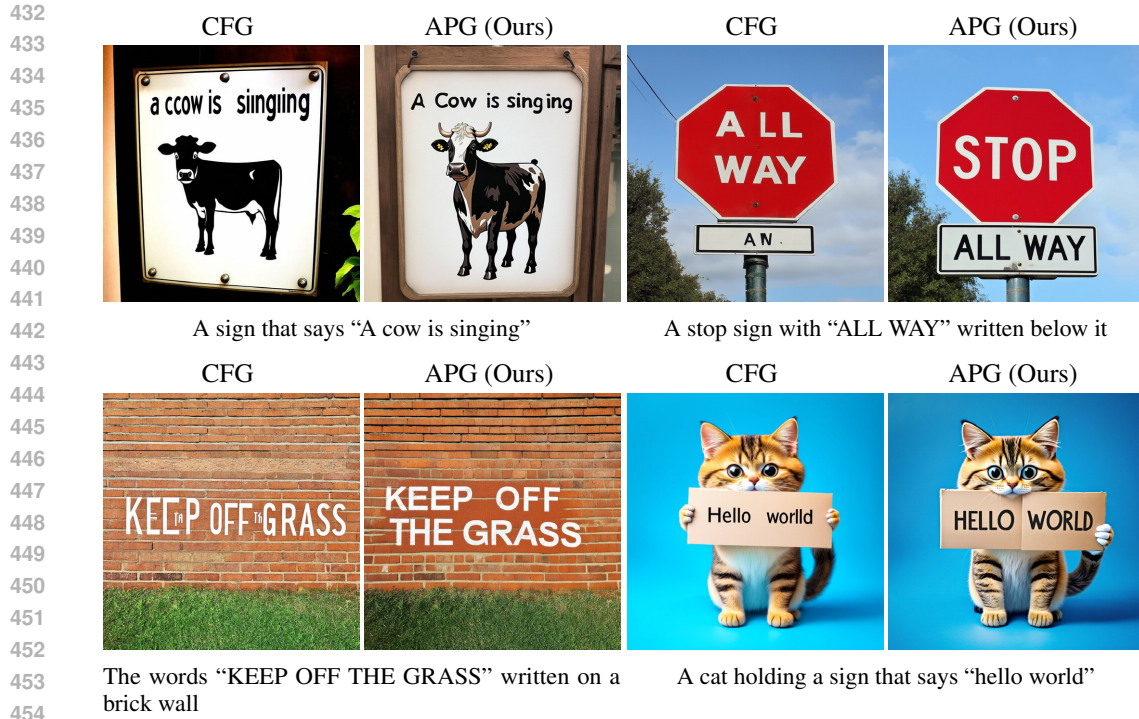


Figure 10: Comparison of CFG and APG for text quality in generated images using Stable Diffusion 3 (Esser et al., 2024). In contrast to CFG, APG consistently produces correct spellings.



Figure 11: Comparison between APG and CFG Rescale using Stable Diffusion XL. CFG Rescale is unable to solve the saturation issue at high guidance scales compared with APG.

Comparison with CFG Rescale CFG Rescale was introduced in (Lin et al., 2024a) as a method to reduce saturation at high guidance scales. In this section, we demonstrate that APG is more effective than CFG Rescale. The comparison in Figure 11 shows that APG outputs have significantly less saturation and are more realistic than those produced with CFG Rescale.

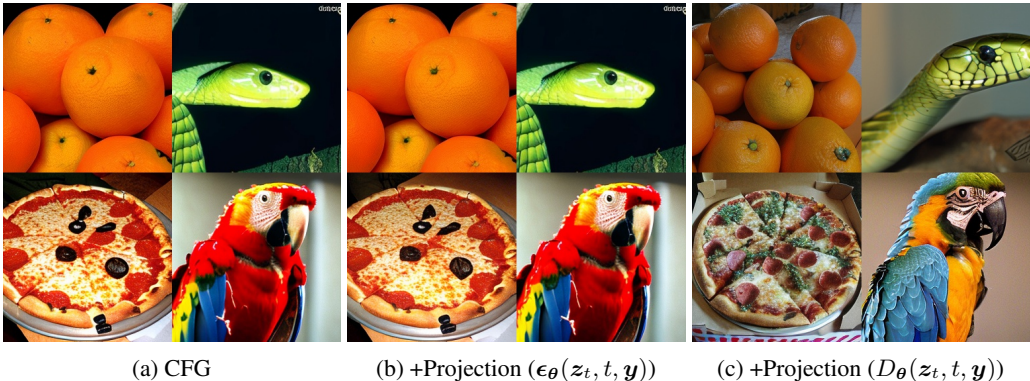


Figure 12: The importance of projecting onto the denoised samples. When performing projection w.r.t. the predicted noise (b), the outputs are barely different than standard CFG (a). However, projecting onto denoised samples (c) more effectively reduces saturation.

Computational cost of APG The computational cost of APG is practically identical to that of CFG, as the rescaling and projection steps incur negligible overhead compared to querying the denoiser. Specifically, in the case of Stable Diffusion XL, the forward pass through the diffusion network takes approximately 130 milliseconds on an RTX 3090 GPU for a single image, while the guidance step requires only about 0.45 milliseconds.

5.2 ABLATION STUDIES

We now present our ablation studies in this section. The experiments are based on class-conditional generation using the EDM2 model (Karras et al., 2023), with FID as the primary metric to justify our design choices. First, Table 2 highlights the importance of each component in APG. We observe that removing projection, rescaling, or reverse momentum results in higher FID scores. Additionally, note that the projection component is primarily responsible for reducing saturation while rescaling and reverse momentum mainly improve FID and recall. Appendix C.8 gives extended ablation results on the effect of each component in APG.

Table 2: Importance of different components in APG.

Config	FID ↓	Recall ↑	Saturation ↓
APG ($w = 4$)	6.49	0.62	0.33
w/o projection	6.63	0.60	0.37
w/o rescaling	7.93	0.56	0.34
w/o momentum	6.85	0.61	0.33

Importance of the model prediction type While CFG works the same across all model prediction types, we observed that our method performs best when applied to the denoised predictions $D_{\theta}(z_t, t, \mathbf{y})$, rather than, for example, the noise prediction $\epsilon_{\theta}(z_t, t, \mathbf{y})$. This is illustrated in Figure 12, where projecting onto $\epsilon_{\theta}(z_t, t, \mathbf{y})$ produces results nearly identical to CFG, while projecting onto $D_{\theta}(z_t, t, \mathbf{y})$ significantly reduces saturation. Note that as discussed in Appendix B, this is not a bottleneck for APG as various prediction types can be readily converted to $D_{\theta}(z_t, t, \mathbf{y})$ at each step.

6 CONCLUSION AND DISCUSSION

In this work, we investigated the oversaturation effect of high CFG scales and introduced a new method, adaptive projected guidance (APG), that achieves the same quality-boosting benefits as CFG without causing oversaturation. The key idea behind APG is to project the CFG update onto the denoised prediction of the diffusion model $D_{\theta}(z_t, t, \mathbf{y})$ and remove or down-weight the component parallel to that prediction. Additionally, by linking CFG to gradient ascent, we demonstrated that its performance can be further enhanced by incorporating rescaling and reverse momentum. Through extensive experiments, we showed that APG improves FID, recall, and saturation metrics compared to CFG, while maintaining similar or better precision. Thus, APG offers a plug-and-play alternative to standard CFG capable of delivering superior results with practically no additional computational overhead. Like CFG, challenges remain in accelerating APG so that the sampling cost approaches that of the unguided sampling (i.e., removing the need to query the diffusion network twice at each sampling step). We consider this a promising direction for future research.

540 ETHICS STATEMENT

541
542 As generative modeling continues to evolve, the potential to create fake or erroneous data increases.
543 While advancements in AI-generated content can enhance efficiency and foster creativity, it is crucial
544 to address the associated ethical concerns. For a more detailed discussion on ethics and creativity in
545 computer vision, we recommend Rostamzadeh et al. (2021).

546 REPRODUCIBILITY STATEMENT

547
548 This work builds on the official implementations of the pretrained models referenced in the main
549 text. The source code for implementing APG is provided in Algorithm 1, and Appendix D outlines
550 additional implementation details, including the hyperparameters used in the main experiments.

551 REFERENCES

- 552
553
554 Mohammadreza Armandpour, Ali Sadeghian, Huangjie Zheng, Amir Sadeghian, and Mingyuan
555 Zhou. Re-imagine the negative prompt algorithm: Transform 2d diffusion into 3d, alleviate janus
556 problem and beyond. *CoRR*, abs/2304.04968, 2023. doi: 10.48550/ARXIV.2304.04968. URL
557 <https://doi.org/10.48550/arXiv.2304.04968>.
- 558
559 Yogesh Balaji, Seungjun Nah, Xun Huang, Arash Vahdat, Jiaming Song, Karsten Kreis, Miika Aittala,
560 Timo Aila, Samuli Laine, Bryan Catanzaro, Tero Karras, and Ming-Yu Liu. ediff-i: Text-to-
561 image diffusion models with an ensemble of expert denoisers. *CoRR*, abs/2211.01324, 2022. doi:
562 10.48550/arXiv.2211.01324. URL <https://doi.org/10.48550/arXiv.2211.01324>.
- 563
564 Andreas Blattmann, Tim Dockhorn, Sumith Kulal, Daniel Mendelevitch, Maciej Kilian, Dominik
565 Lorenz, Yam Levi, Zion English, Vikram Voleti, Adam Letts, Varun Jampani, and Robin Rom-
566 bach. Stable video diffusion: Scaling latent video diffusion models to large datasets. *CoRR*,
567 abs/2311.15127, 2023a. doi: 10.48550/ARXIV.2311.15127. URL [https://doi.org/10.48550/arXiv.](https://doi.org/10.48550/arXiv.2311.15127)
568 [2311.15127](https://doi.org/10.48550/arXiv.2311.15127).
- 569
570 Andreas Blattmann, Robin Rombach, Huan Ling, Tim Dockhorn, Seung Wook Kim, Sanja Fidler, and
571 Karsten Kreis. Align your latents: High-resolution video synthesis with latent diffusion models.
572 In *Proceedings of the IEEE/CVF Conference on Computer Vision and Pattern Recognition*, pp.
22563–22575, 2023b.
- 573
574 Andrew Brock, Jeff Donahue, and Karen Simonyan. Large scale GAN training for high fidelity
575 natural image synthesis. In *7th International Conference on Learning Representations, ICLR*
576 *2019, New Orleans, LA, USA, May 6-9, 2019*. OpenReview.net, 2019. URL [https://openreview.net/](https://openreview.net/forum?id=B1xsqj09Fm)
577 [forum?id=B1xsqj09Fm](https://openreview.net/forum?id=B1xsqj09Fm).
- 578
579 Junsong Chen, Yue Wu, Simian Luo, Enze Xie, Sayak Paul, Ping Luo, Hang Zhao, and Zhenguo Li.
580 Pixart- δ : Fast and controllable image generation with latent consistency models. *arXiv*
preprint arXiv:2401.05252, 2024.
- 581
582 Nanxin Chen, Yu Zhang, Heiga Zen, Ron J. Weiss, Mohammad Norouzi, and William Chan. Wave-
583 rad: Estimating gradients for waveform generation. In *9th International Conference on Learning*
584 *Representations, ICLR 2021, Virtual Event, Austria, May 3-7, 2021*. OpenReview.net, 2021. URL
585 <https://openreview.net/forum?id=NsMLjcFaO8O>.
- 586
587 Prafulla Dhariwal and Alexander Quinn Nichol. Diffusion models beat gans on image synthe-
588 sis. In Marc’Aurelio Ranzato, Alina Beygelzimer, Yann N. Dauphin, Percy Liang, and Jen-
589 nifer Wortman Vaughan (eds.), *Advances in Neural Information Processing Systems 34: An-
590 nual Conference on Neural Information Processing Systems 2021, NeurIPS 2021, December*
591 *6-14, 2021, virtual*, pp. 8780–8794, 2021. URL [https://proceedings.neurips.cc/paper/2021/hash/](https://proceedings.neurips.cc/paper/2021/hash/49ad23d1ec9fa4bd8d77d02681df5cfa-Abstract.html)
[49ad23d1ec9fa4bd8d77d02681df5cfa-Abstract.html](https://proceedings.neurips.cc/paper/2021/hash/49ad23d1ec9fa4bd8d77d02681df5cfa-Abstract.html).
- 592
593 Patrick Esser, Sumith Kulal, Andreas Blattmann, Rahim Entezari, Jonas Müller, Harry Saini, Yam
Levi, Dominik Lorenz, Axel Sauer, Frederic Boesel, et al. Scaling rectified flow transformers for
high-resolution image synthesis. *arXiv preprint arXiv:2403.03206*, 2024.

- 594 Agrim Gupta, Lijun Yu, Kihyuk Sohn, Xiuye Gu, Meera Hahn, Li Fei-Fei, Irfan Essa, Lu Jiang,
595 and José Lezama. Photorealistic video generation with diffusion models. *arXiv preprint*
596 *arXiv:2312.06662*, 2023.
- 597
598 Martin Heusel, Hubert Ramsauer, Thomas Unterthiner, Bernhard Nessler, and Sepp Hochreiter.
599 Gans trained by a two time-scale update rule converge to a local nash equilibrium. In Isabelle
600 Guyon, Ulrike von Luxburg, Samy Bengio, Hanna M. Wallach, Rob Fergus, S. V. N. Vish-
601 wanathan, and Roman Garnett (eds.), *Advances in Neural Information Processing Systems 30:*
602 *Annual Conference on Neural Information Processing Systems 2017, December 4-9, 2017, Long*
603 *Beach, CA, USA*, pp. 6626–6637, 2017. URL [https://proceedings.neurips.cc/paper/2017/hash/](https://proceedings.neurips.cc/paper/2017/hash/8a1d694707eb0fefe65871369074926d-Abstract.html)
604 [8a1d694707eb0fefe65871369074926d-Abstract.html](https://proceedings.neurips.cc/paper/2017/hash/8a1d694707eb0fefe65871369074926d-Abstract.html).
- 605 Jonathan Ho and Tim Salimans. Classifier-free diffusion guidance. *CoRR*, abs/2207.12598, 2022.
606 doi: 10.48550/arXiv.2207.12598. URL <https://doi.org/10.48550/arXiv.2207.12598>.
- 607
608 Jonathan Ho, Ajay Jain, and Pieter Abbeel. Denoising diffusion probabilistic models. In Hugo
609 Larochelle, Marc Aurelio Ranzato, Raia Hadsell, Maria-Florina Balcan, and Hsuan-Tien Lin (eds.),
610 *Advances in Neural Information Processing Systems 33: Annual Conference on Neural Information*
611 *Processing Systems 2020, NeurIPS 2020, December 6-12, 2020, virtual*, 2020. URL [https:](https://proceedings.neurips.cc/paper/2020/hash/4c5bcfec8584af0d967f1ab10179ca4b-Abstract.html)
612 [//proceedings.neurips.cc/paper/2020/hash/4c5bcfec8584af0d967f1ab10179ca4b-Abstract.html](https://proceedings.neurips.cc/paper/2020/hash/4c5bcfec8584af0d967f1ab10179ca4b-Abstract.html).
- 613 Emiel Hoogeboom, Jonathan Heek, and Tim Salimans. simple diffusion: End-to-end diffusion for
614 high resolution images. *CoRR*, abs/2301.11093, 2023. doi: 10.48550/arXiv.2301.11093. URL
615 <https://doi.org/10.48550/arXiv.2301.11093>.
- 616 Qingqing Huang, Daniel S. Park, Tao Wang, Timo I. Denk, Andy Ly, Nanxin Chen, Zhengdong
617 Zhang, Zhishuai Zhang, Jiahui Yu, Christian Havnø Frank, Jesse H. Engel, Quoc V. Le, William
618 Chan, and Wei Han. Noise2music: Text-conditioned music generation with diffusion models.
619 *CoRR*, abs/2302.03917, 2023. doi: 10.48550/arXiv.2302.03917. URL [https://doi.org/10.48550/](https://doi.org/10.48550/arXiv.2302.03917)
620 [arXiv.2302.03917](https://doi.org/10.48550/arXiv.2302.03917).
- 621 Tero Karras, Miika Aittala, Timo Aila, and Samuli Laine. Elucidating the design space of diffusion-
622 based generative models. 2022. URL <https://openreview.net/forum?id=k7FuTOWMOc7>.
- 623
624 Tero Karras, Miika Aittala, Jaakko Lehtinen, Janne Hellsten, Timo Aila, and Samuli Laine. Analyzing
625 and improving the training dynamics of diffusion models, 2023.
- 626
627 Diederik P. Kingma and Ruiqi Gao. Vdm++: Variational diffusion models for high-quality synthesis,
628 2023.
- 629 Zhifeng Kong, Wei Ping, Jiaji Huang, Kexin Zhao, and Bryan Catanzaro. Diffwave: A versatile
630 diffusion model for audio synthesis. In *9th International Conference on Learning Representations,*
631 *ICLR 2021, Virtual Event, Austria, May 3-7, 2021*. OpenReview.net, 2021. URL [https://openreview.](https://openreview.net/forum?id=a-xFK8Ymz5J)
632 [net/forum?id=a-xFK8Ymz5J](https://openreview.net/forum?id=a-xFK8Ymz5J).
- 633
634 Tuomas Kynkäänniemi, Tero Karras, Samuli Laine, Jaakko Lehtinen, and Timo Aila. Im-
635 proved precision and recall metric for assessing generative models. In Hanna M. Wallach,
636 Hugo Larochelle, Alina Beygelzimer, Florence d’Alché-Buc, Emily B. Fox, and Roman Gar-
637 nett (eds.), *Advances in Neural Information Processing Systems 32: Annual Conference on*
638 *Neural Information Processing Systems 2019, NeurIPS 2019, December 8-14, 2019, Vancou-*
639 *ver, BC, Canada*, pp. 3929–3938, 2019. URL [https://proceedings.neurips.cc/paper/2019/hash/](https://proceedings.neurips.cc/paper/2019/hash/0234c510bc6d908b28c70ff313743079-Abstract.html)
640 [0234c510bc6d908b28c70ff313743079-Abstract.html](https://proceedings.neurips.cc/paper/2019/hash/0234c510bc6d908b28c70ff313743079-Abstract.html).
- 641
642 Tuomas Kynkäänniemi, Miika Aittala, Tero Karras, Samuli Laine, Timo Aila, and Jaakko Lehtinen.
643 Applying guidance in a limited interval improves sample and distribution quality in diffusion
644 models. *CoRR*, abs/2404.07724, 2024. doi: 10.48550/ARXIV.2404.07724. URL [https://doi.org/](https://doi.org/10.48550/arXiv.2404.07724)
[10.48550/arXiv.2404.07724](https://doi.org/10.48550/arXiv.2404.07724).
- 645
646 Shanchuan Lin, Bingchen Liu, Jiashi Li, and Xiao Yang. Common diffusion noise schedules
647 and sample steps are flawed. In *IEEE/CVF Winter Conference on Applications of Computer*
Vision, WACV 2024, Waikoloa, HI, USA, January 3-8, 2024, pp. 5392–5399. IEEE, 2024a. doi:
10.1109/WACV57701.2024.00532. URL <https://doi.org/10.1109/WACV57701.2024.00532>.

- 648 Shanchuan Lin, Anran Wang, and Xiao Yang. Sd-xl-lightning: Progressive adversarial diffusion
649 distillation. *arXiv preprint arXiv:2402.13929*, 2024b.
- 650
- 651 Shanchuan Lin, Anran Wang, and Xiao Yang. Sd-xl-lightning: Progressive adversarial diffusion
652 distillation. *CoRR*, abs/2402.13929, 2024c. doi: 10.48550/ARXIV.2402.13929. URL <https://doi.org/10.48550/arXiv.2402.13929>.
- 653
- 654 Tsung-Yi Lin, Michael Maire, Serge J. Belongie, James Hays, Pietro Perona, Deva Ramanan, Piotr
655 Dollár, and C. Lawrence Zitnick. Microsoft COCO: common objects in context. In David J.
656 Fleet, Tomás Pajdla, Bernt Schiele, and Tinne Tuytelaars (eds.), *Computer Vision - ECCV 2014*
657 - *13th European Conference, Zurich, Switzerland, September 6-12, 2014, Proceedings, Part V*,
658 volume 8693 of *Lecture Notes in Computer Science*, pp. 740–755. Springer, 2014. doi: 10.1007/
659 978-3-319-10602-1_48. URL https://doi.org/10.1007/978-3-319-10602-1_48.
- 660
- 661 Guan-Hong Liu, Arash Vahdat, De-An Huang, Evangelos A. Theodorou, Weili Nie, and Anima
662 Anandkumar. I²sb: Image-to-image schrödinger bridge. *CoRR*, abs/2302.05872, 2023a. doi:
663 10.48550/arXiv.2302.05872. URL <https://doi.org/10.48550/arXiv.2302.05872>.
- 664
- 665 Luping Liu, Yi Ren, Zhijie Lin, and Zhou Zhao. Pseudo numerical methods for diffusion models on
666 manifolds. 2022a. URL <https://openreview.net/forum?id=PIKWVd2yBkY>.
- 667
- 668 Luping Liu, Yi Ren, Zhijie Lin, and Zhou Zhao. Pseudo numerical methods for diffusion models
669 on manifolds. In *The Tenth International Conference on Learning Representations, ICLR 2022,*
670 *Virtual Event, April 25-29, 2022*. OpenReview.net, 2022b. URL <https://openreview.net/forum?id=PIKWVd2yBkY>.
- 671
- 672 Xingchao Liu, Chengyue Gong, and Qiang Liu. Flow straight and fast: Learning to generate and
673 transfer data with rectified flow. 2023b. URL <https://openreview.net/forum?id=XVjTT1nw5z>.
- 674
- 675 Cheng Lu, Yuhao Zhou, Fan Bao, Jianfei Chen, Chongxuan Li, and Jun Zhu. Dpm-
676 solver: A fast ODE solver for diffusion probabilistic model sampling in around
677 10 steps. In *NeurIPS*, 2022a. URL http://papers.nips.cc/paper_files/paper/2022/hash/260a14acce2a89dad36adc8eefe7c59e-Abstract-Conference.html.
- 678
- 679 Cheng Lu, Yuhao Zhou, Fan Bao, Jianfei Chen, Chongxuan Li, and Jun Zhu. Dpm-solver++: Fast
680 solver for guided sampling of diffusion probabilistic models. *CoRR*, abs/2211.01095, 2022b. doi:
681 10.48550/arXiv.2211.01095. URL <https://doi.org/10.48550/arXiv.2211.01095>.
- 682
- 683 Kevin P. Murphy. *Probabilistic Machine Learning: Advanced Topics*. MIT Press, 2023. URL
684 <http://probml.github.io/book2>.
- 685
- 686 Alexander Quinn Nichol and Prafulla Dhariwal. Improved denoising diffusion probabilistic models.
687 In Marina Meila and Tong Zhang (eds.), *Proceedings of the 38th International Conference on*
688 *Machine Learning, ICML 2021, 18-24 July 2021, Virtual Event*, volume 139 of *Proceedings of*
689 *Machine Learning Research*, pp. 8162–8171. PMLR, 2021. URL <http://proceedings.mlr.press/v139/nichol21a.html>.
- 690
- 691 Alexander Quinn Nichol, Prafulla Dhariwal, Aditya Ramesh, Pranav Shyam, Pamela Mishkin, Bob
692 McGrew, Ilya Sutskever, and Mark Chen. GLIDE: towards photorealistic image generation and
693 editing with text-guided diffusion models. In Kamalika Chaudhuri, Stefanie Jegelka, Le Song,
694 Csaba Szepesvári, Gang Niu, and Sivan Sabato (eds.), *International Conference on Machine*
695 *Learning, ICML 2022, 17-23 July 2022, Baltimore, Maryland, USA*, volume 162 of *Proceedings of*
696 *Machine Learning Research*, pp. 16784–16804. PMLR, 2022. URL <https://proceedings.mlr.press/v162/nichol22a.html>.
- 697
- 698 William Peebles and Saining Xie. Scalable diffusion models with transformers. *CoRR*,
699 abs/2212.09748, 2022. doi: 10.48550/arXiv.2212.09748. URL <https://doi.org/10.48550/arXiv.2212.09748>.
- 700
- 701 Dustin Podell, Zion English, Kyle Lacey, Andreas Blattmann, Tim Dockhorn, Jonas Müller, Joe
Penna, and Robin Rombach. SDXL: improving latent diffusion models for high-resolution
image synthesis. *CoRR*, abs/2307.01952, 2023. doi: 10.48550/ARXIV.2307.01952. URL <https://doi.org/10.48550/arXiv.2307.01952>.

- 702 Aditya Ramesh, Prafulla Dhariwal, Alex Nichol, Casey Chu, and Mark Chen. Hierarchical text-
703 conditional image generation with CLIP latents. *CoRR*, abs/2204.06125, 2022. doi: 10.48550/
704 arXiv.2204.06125. URL [https://doi.org/10.48550/
705 arXiv.2204.06125](https://doi.org/10.48550/arXiv.2204.06125).
- 706 Robin Rombach, Andreas Blattmann, Dominik Lorenz, Patrick Esser, and Björn Ommer. High-
707 resolution image synthesis with latent diffusion models. In *IEEE/CVF Conference on Computer
708 Vision and Pattern Recognition, CVPR 2022, New Orleans, LA, USA, June 18-24, 2022*, pp.
709 10674–10685. IEEE, 2022. doi: 10.1109/CVPR52688.2022.01042. URL [https://doi.org/10.1109/
711 CVPR52688.2022.01042](https://doi.org/10.1109/
710 CVPR52688.2022.01042).
- 712 Negar Rostamzadeh, Emily Denton, and Linda Petrini. Ethics and creativity in computer vision.
713 *CoRR*, abs/2112.03111, 2021. URL <https://arxiv.org/abs/2112.03111>.
- 714 Olga Russakovsky, Jia Deng, Hao Su, Jonathan Krause, Sanjeev Satheesh, Sean Ma, Zhiheng
715 Huang, Andrej Karpathy, Aditya Khosla, Michael S. Bernstein, Alexander C. Berg, and Li Fei-Fei.
716 Imagenet large scale visual recognition challenge. *Int. J. Comput. Vis.*, 115(3):211–252, 2015. doi:
717 10.1007/s11263-015-0816-y. URL <https://doi.org/10.1007/s11263-015-0816-y>.
- 718 Seyedmorteza Sadat, Jakob Buhmann, Derek Bradley, Otmar Hilliges, and Romann M. Weber. CADs:
719 Unleashing the diversity of diffusion models through condition-annealed sampling. In *The Twelfth
720 International Conference on Learning Representations*, 2024a. URL [https://openreview.net/forum?
722 id=zMoNrajk2X](https://openreview.net/forum?
721 id=zMoNrajk2X).
- 723 Seyedmorteza Sadat, Manuel Kansy, Otmar Hilliges, and Romann M Weber. No training, no problem:
724 Rethinking classifier-free guidance for diffusion models. *arXiv preprint arXiv:2407.02687*, 2024b.
725
- 726 Chitwan Saharia, William Chan, Huiwen Chang, Chris A. Lee, Jonathan Ho, Tim Salimans, David J.
727 Fleet, and Mohammad Norouzi. Palette: Image-to-image diffusion models. In Munkhtsetseg
728 Nandigjavi, Niloy J. Mitra, and Aaron Hertzmann (eds.), *SIGGRAPH '22: Special Interest Group
729 on Computer Graphics and Interactive Techniques Conference, Vancouver, BC, Canada, August 7 -
730 11, 2022*, pp. 15:1–15:10. ACM, 2022a. doi: 10.1145/3528233.3530757. URL [https://doi.org/10.
732 1145/3528233.3530757](https://doi.org/10.
731 1145/3528233.3530757).
- 733 Chitwan Saharia, William Chan, Saurabh Saxena, Lala Li, Jay Whang, Emily L. Denton, Seyed Kam-
734 yar Seyed Ghasemipour, Raphael Gontijo Lopes, Burcu Karagol Ayan, Tim Salimans, Jonathan
735 Ho, David J. Fleet, and Mohammad Norouzi. Photorealistic text-to-image diffusion models with
736 deep language understanding. 2022b. URL [http://papers.nips.cc/paper_files/paper/2022/hash/
738 ec795aeadae0b7d230fa35cbaf04c041-Abstract-Conference.html](http://papers.nips.cc/paper_files/paper/2022/hash/
737 ec795aeadae0b7d230fa35cbaf04c041-Abstract-Conference.html).
- 739 Tim Salimans and Jonathan Ho. Progressive distillation for fast sampling of diffusion models. In
740 *The Tenth International Conference on Learning Representations, ICLR 2022, Virtual Event, April
741 25-29, 2022*. OpenReview.net, 2022. URL <https://openreview.net/forum?id=TIIdIXIpzhoI>.
- 742 sd community. Sdxl flash in collaboration with project fluently. [https://huggingface.co/sd-community/
744 sdxl-flash](https://huggingface.co/sd-community/
743 sdxl-flash). Accessed: 2024-09-08.
- 745 Jascha Sohl-Dickstein, Eric A. Weiss, Niru Maheswaranathan, and Surya Ganguli. Deep unsupervised
746 learning using nonequilibrium thermodynamics. 37:2256–2265, 2015. URL [http://proceedings.
748 mlr.press/v37/sohl-dickstein15.html](http://proceedings.
747 mlr.press/v37/sohl-dickstein15.html).
- 749 Jiaming Song, Chenlin Meng, and Stefano Ermon. Denoising diffusion implicit models. In *9th
750 International Conference on Learning Representations, ICLR 2021, Virtual Event, Austria, May
751 3-7, 2021*. OpenReview.net, 2021a. URL <https://openreview.net/forum?id=St1giarCHLP>.
- 752 Yang Song and Stefano Ermon. Generative modeling by estimating gradients of the data distribution.
753 In Hanna M. Wallach, Hugo Larochelle, Alina Beygelzimer, Florence d’Alché-Buc, Emily B.
754 Fox, and Roman Garnett (eds.), *Advances in Neural Information Processing Systems 32: Annual
755 Conference on Neural Information Processing Systems 2019, NeurIPS 2019, December 8-14, 2019,
Vancouver, BC, Canada*, pp. 11895–11907, 2019. URL [https://proceedings.neurips.cc/paper/2019/
hash/3001ef257407d5a371a96dcd947c7d93-Abstract.html](https://proceedings.neurips.cc/paper/2019/
hash/3001ef257407d5a371a96dcd947c7d93-Abstract.html).

756 Yang Song, Jascha Sohl-Dickstein, Diederik P. Kingma, Abhishek Kumar, Stefano Ermon, and
757 Ben Poole. Score-based generative modeling through stochastic differential equations. In *9th*
758 *International Conference on Learning Representations, ICLR 2021, Virtual Event, Austria, May*
759 *3-7, 2021*. OpenReview.net, 2021b. URL <https://openreview.net/forum?id=PxTIG12RRHS>.
760

761 Jiahui Yu, Yuanzhong Xu, Jing Yu Koh, Thang Luong, Gunjan Baid, Zirui Wang, Vijay Vasudevan,
762 Alexander Ku, Yinfei Yang, Burcu Karagol Ayan, Ben Hutchinson, Wei Han, Zarana Parekh, Xin
763 Li, Han Zhang, Jason Baldridge, and Yonghui Wu. Scaling autoregressive models for content-rich
764 text-to-image generation. *Trans. Mach. Learn. Res.*, 2022, 2022. URL [https://openreview.net/](https://openreview.net/forum?id=AFDcYJKhND)
765 [forum?id=AFDcYJKhND](https://openreview.net/forum?id=AFDcYJKhND).
766

767 Wenliang Zhao, Lujia Bai, Yongming Rao, Jie Zhou, and Jiwen Lu. Unipc: A unified predictor-
768 corrector framework for fast sampling of diffusion models. *CoRR*, abs/2302.04867, 2023. doi:
769 10.48550/arXiv.2302.04867. URL <https://doi.org/10.48550/arXiv.2302.04867>.
770

771 Candi Zheng and Yuan Lan. Characteristic guidance: Non-linear correction for diffusion model at
772 large guidance scale. 2024. URL <https://openreview.net/forum?id=eOtgMYdGLt>.
773
774
775
776
777
778
779
780
781
782
783
784
785
786
787
788
789
790
791
792
793
794
795
796
797
798
799
800
801
802
803
804
805
806
807
808
809

A DETAILS ON CFG AS GRADIENT ASCENT

In this section, we discuss how CFG can be interpreted as one step of gradient ascent. To begin, note that the CFG update rule can be expressed as:

$$\hat{D}_{\text{CFG}}(\mathbf{z}_t, t, \mathbf{y}) = D_{\theta}(\mathbf{z}_t, t, \mathbf{y}_{\text{null}}) + w(D_{\theta}(\mathbf{z}_t, t, \mathbf{y}) - D_{\theta}(\mathbf{z}_t, t, \mathbf{y}_{\text{null}})) \quad (7)$$

$$= wD_{\theta}(\mathbf{z}_t, t, \mathbf{y}) + (1 - w)D_{\theta}(\mathbf{z}_t, t, \mathbf{y}_{\text{null}}) \quad (8)$$

$$= D_{\theta}(\mathbf{z}_t, t, \mathbf{y}) + (w - 1)D_{\theta}(\mathbf{z}_t, t, \mathbf{y}) + (1 - w)D_{\theta}(\mathbf{z}_t, t, \mathbf{y}_{\text{null}}) \quad (9)$$

$$= D_{\theta}(\mathbf{z}_t, t, \mathbf{y}) + (w - 1)(D_{\theta}(\mathbf{z}_t, t, \mathbf{y}) - D_{\theta}(\mathbf{z}_t, t, \mathbf{y}_{\text{null}})) \quad (10)$$

$$= D_{\theta}(\mathbf{z}_t, t, \mathbf{y}) + \gamma \Delta D_t, \quad (11)$$

where $\gamma = w - 1$, and $\Delta D_t = D_{\theta}(\mathbf{z}_t, t, \mathbf{y}) - D_{\theta}(\mathbf{z}_t, t, \mathbf{y}_{\text{null}})$. Next, observe that we can write:

$$D_{\theta}(\mathbf{z}_t, t, \mathbf{y}) - D_{\theta}(\mathbf{z}_t, t, \mathbf{y}_{\text{null}}) = \nabla_{D_{\theta}(\mathbf{z}_t, t, \mathbf{y})} \left[\frac{1}{2} \|D_{\theta}(\mathbf{z}_t, t, \mathbf{y}) - D_{\theta}(\mathbf{z}_t, t, \mathbf{y}_{\text{null}})\|^2 \right]. \quad (12)$$

Thus, if we define the CFG objective function as

$$f_{\text{CFG}}(D_{\theta}(\mathbf{z}_t, t, \mathbf{y}), D_{\theta}(\mathbf{z}_t, t, \mathbf{y}_{\text{null}})) = \frac{1}{2} \|D_{\theta}(\mathbf{z}_t, t, \mathbf{y}) - D_{\theta}(\mathbf{z}_t, t, \mathbf{y}_{\text{null}})\|^2, \quad (13)$$

the CFG update rule becomes equivalent to:

$$\hat{D}_{\text{CFG}}(\mathbf{z}_t, t, \mathbf{y}) = D_{\theta}(\mathbf{z}_t, t, \mathbf{y}) + \gamma \nabla_{D_{\theta}(\mathbf{z}_t, t, \mathbf{y})} f_{\text{CFG}}(D_{\theta}(\mathbf{z}_t, t, \mathbf{y}), D_{\theta}(\mathbf{z}_t, t, \mathbf{y}_{\text{null}})). \quad (14)$$

Hence, we have shown that the CFG update rule corresponds to a single step of gradient *ascent* with respect to the objective function $f_{\text{CFG}}(D_{\theta}(\mathbf{z}_t, t, \mathbf{y}), D_{\theta}(\mathbf{z}_t, t, \mathbf{y}_{\text{null}}))$.

This interpretation motivated us to incorporate rescaling into standard CFG. Since the objective function $f_{\text{CFG}}(D_{\theta}(\mathbf{z}_t, t, \mathbf{y}), D_{\theta}(\mathbf{z}_t, t, \mathbf{y}_{\text{null}}))$ does not have a maximum, the CFG update step may result in arbitrary drift from $D_{\theta}(\mathbf{z}_t, t, \mathbf{y})$. By applying rescaling, we constrain the CFG update to remain within a ball of limited radius around $D_{\theta}(\mathbf{z}_t, t, \mathbf{y})$. The reverse momentum method is similarly inspired by this interpretation, where each update is pushed away from previous predictions.

B DENOISED PREDICTION FOR DIFFERENT DIFFUSION MODELS

We next briefly outline the process of computing the denoised prediction $D_{\theta}(\mathbf{z}_t, t, \mathbf{y})$ for various diffusion models. For further details, we refer readers to [Kingma & Gao \(2023\)](#). In the following, let \mathbf{x} represent the clean data, \mathbf{y} a condition or class, and $\epsilon \sim \mathcal{N}(\mathbf{0}, \mathbf{I})$ the noise. Given a noisy sample \mathbf{z}_t at time step t , the objective is to recover the clean data \mathbf{x} that produced \mathbf{z}_t . The denoised version of \mathbf{z}_t , which approximates \mathbf{x} , is estimated by a neural network, denoted as $D_{\theta}(\mathbf{z}_t, t, \mathbf{y})$. Before applying APG, we always convert all model predictions to $D_{\theta}(\mathbf{z}_t, t, \mathbf{y})$. This conversion is compatible with most samplers based on the denoising framework, such as EDM ([Karras et al., 2022](#)) and DPM++ ([Lu et al., 2022b](#)). The conversions for various models are derived below, and a summary is provided in Table 3.

DDPM For models using the DDPM framework ([Ho et al., 2020](#)), the forward diffusion process is defined as $\mathbf{z}_t = \alpha_t \mathbf{x} + \sigma_t \epsilon$, where $\sigma_t^2 + \alpha_t^2 = 1$. These models typically predict the total added noise ϵ via a neural network $\epsilon_{\theta}(\mathbf{z}_t, t, \mathbf{y})$. Given the prediction of the model, the denoised prediction can be estimated via

$$D_{\theta}(\mathbf{z}_t, t, \mathbf{y}) = \frac{\mathbf{z}_t - \sigma_t \epsilon_{\theta}(\mathbf{z}_t, t, \mathbf{y})}{\alpha_t}. \quad (15)$$

If the model predicts the velocity $\mathbf{v} = \alpha_t \epsilon - \sigma_t \mathbf{x}$, we have

$$\mathbf{v} = \alpha_t \frac{\mathbf{z}_t - \alpha_t \mathbf{x}}{\sigma_t} - \sigma_t \mathbf{x} = \frac{\alpha_t \mathbf{z}_t - \alpha_t^2 \mathbf{x} - \sigma_t^2 \mathbf{x}}{\sigma_t} = \frac{\alpha_t \mathbf{z}_t - \mathbf{x}}{\sigma_t}. \quad (16)$$

This leads to the following formulation for the denoised prediction:

$$D_{\theta}(\mathbf{z}_t, t, \mathbf{y}) = \alpha_t \mathbf{z}_t - \sigma_t \mathbf{v}_{\theta}(\mathbf{z}_t, t, \mathbf{y}). \quad (17)$$

Table 3: Summary of calculating denoised predictions $D_{\theta}(\mathbf{z}_t, t, \mathbf{y})$ for different diffusion models.

Config	Forward process \mathbf{z}_t	Model prediction	Denoised prediction $D_{\theta}(\mathbf{z}_t, t, \mathbf{y})$
DDPM	$\alpha_t \mathbf{x} + \sigma_t \epsilon$	$\epsilon_{\theta}(\mathbf{z}_t, t, \mathbf{y})$	$(\mathbf{z}_t - \sigma_t \epsilon_{\theta}(\mathbf{z}_t, t, \mathbf{y})) / \alpha_t$
DDPM	$\alpha_t \mathbf{x} + \sigma_t \epsilon$	$\mathbf{v}_{\theta}(\mathbf{z}_t, t, \mathbf{y})$	$\alpha_t \mathbf{z}_t - \sigma_t \mathbf{v}_{\theta}(\mathbf{z}_t, t, \mathbf{y})$
EDM	$\mathbf{x} + \sigma(t) \epsilon$	$F_{\theta}(c_{\text{in}}(t) \mathbf{z}_t, c_{\text{noise}}(t), \mathbf{y})$	$c_{\text{skip}}(t) \mathbf{z}_t + c_{\text{out}}(t) F_{\theta}(c_{\text{in}}(t) \mathbf{z}_t, c_{\text{noise}}(t), \mathbf{y})$
Rectified flow	$(1-t)\mathbf{x} + t\epsilon$	$\mathbf{v}_{\theta}(\mathbf{z}_t, t, \mathbf{y})$	$\mathbf{z}_t - t \mathbf{v}_{\theta}(\mathbf{z}_t, t, \mathbf{y})$

EDM framework For the EDM framework (Karras et al., 2022), the forward process is described by $\mathbf{z}_t = \mathbf{x} + \sigma(t)\epsilon$, and the denoised prediction $D_{\theta}(\mathbf{z}_t, t, \mathbf{y})$ is formulated via

$$D_{\theta}(\mathbf{z}_t, t, \mathbf{y}) = c_{\text{skip}}(t) \mathbf{z}_t + c_{\text{out}}(t) F_{\theta}(c_{\text{in}}(t) \mathbf{z}_t, c_{\text{noise}}(t), \mathbf{y}), \quad (18)$$

where $F_{\theta}(c_{\text{in}}(t) \mathbf{z}_t, c_{\text{noise}}(t), \mathbf{y})$ is the output of the neural network. The EDM framework uses $\sigma(t) \propto t$; thus, σ and t can be used interchangeably in this framework.

Rectified flow models For rectified flow models (Liu et al., 2023b), such as Stable Diffusion 3 (Esser et al., 2024), the forward process is given by $\mathbf{z}_t = (1-t)\mathbf{x} + t\epsilon$. The model predicts the velocity field given by $\mathbf{v} = \epsilon - \mathbf{x}$. Accordingly, we have

$$\mathbf{v} = \epsilon - \mathbf{x} = \frac{\mathbf{z}_t - (1-t)\mathbf{x}}{t} - \mathbf{x} = \frac{\mathbf{z}_t - (1-t)\mathbf{x} - t\mathbf{x}}{t} = \frac{\mathbf{z}_t - \mathbf{x}}{t}. \quad (19)$$

Thus, the denoised prediction can be determined by:

$$D_{\theta}(\mathbf{z}_t, t, \mathbf{y}) = \mathbf{z}_t - t \mathbf{v}_{\theta}(\mathbf{z}_t, t, \mathbf{y}) = \mathbf{z}_t - \sigma_t \mathbf{v}_{\theta}(\mathbf{z}_t, t, \mathbf{y}), \quad (20)$$

where we define $\sigma_t = t$.

This section demonstrates the effect of applying APG on a toy example to illustrate the differences between APG and CFG. We use a mixture of two high-dimensional Gaussians as the data distribution, which allows us to analytically compute the score functions during the diffusion process, eliminating potential errors introduced by a denoiser network. Specifically, the data distribution p_{data} is defined as:

$$p_{\text{data}}(\mathbf{x}) = \frac{1}{2} \mathcal{N}(\boldsymbol{\mu}_1, \sigma^2 \mathbf{I})(\mathbf{x}) + \frac{1}{2} \mathcal{N}(\boldsymbol{\mu}_2, \sigma^2 \mathbf{I})(\mathbf{x}), \quad (21)$$

where $\boldsymbol{\mu}_1 = [-2, -2, \dots, -2]$, $\boldsymbol{\mu}_2 = [2, 2, \dots, 2]$, and $\sigma = 0.25$. We use a dimensionality of 500 for each component. Accordingly, the conditional distributions are equal to

$$p_{\text{data}}(\mathbf{x} | y = 1) = \mathcal{N}(\boldsymbol{\mu}_1, \sigma^2 \mathbf{I})(\mathbf{x}) \quad \text{and} \quad p_{\text{data}}(\mathbf{x} | y = 2) = \mathcal{N}(\boldsymbol{\mu}_2, \sigma^2 \mathbf{I})(\mathbf{x}). \quad (22)$$

The sampling results are shown in Figure 13 (visualizing the first two dimensions of each Gaussian). When CFG is applied with a high guidance scale, it results in a drift toward regions less likely according to the data distribution. In contrast, applying APG corrects this drift and improves mode coverage. While this is a simplified example, we argue that a similar phenomenon occurs when applying CFG to images, leading to artifacts and oversaturation in the final outputs.

C ADDITIONAL EXPERIMENTS

Additional experiments and ablation studies are included in this section. Unless stated otherwise, the experiments are conducted using class-conditional ImageNet (Russakovsky et al., 2015) generation.

C.1 COMPATIBILITY WITH CADS AND IG

We first demonstrate that APG is compatible with CADS (Sadat et al., 2024a) and interval guidance (IG) (Kynkäänniemi et al., 2024), both of which are designed to enhance the diversity of generations at high guidance scales. The results, shown in Table 4, indicate that replacing CFG with APG leads to improved FID, recall, and saturation scores for both methods.

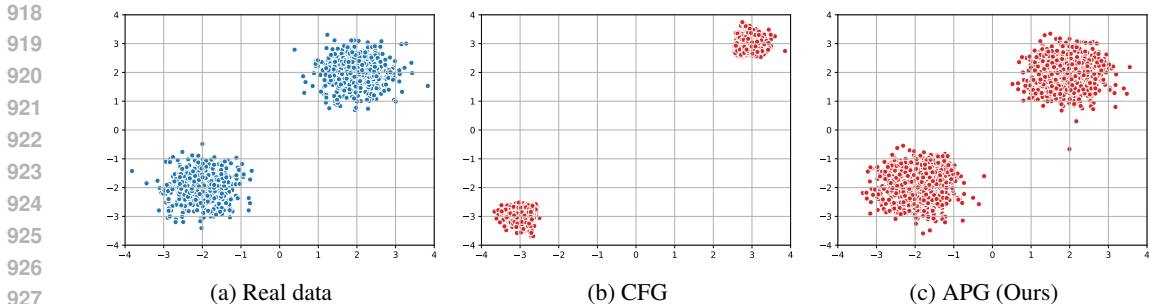


Figure 13: Visualizing the effect of APG on the sampling process using a toy problem. The real samples from the data distribution are shown in (a). When sampling with high guidance, CFG leads to a drift away from the true mean of the data distribution and results in reduced mode coverage in the generated samples (b). In contrast, sampling with APG eliminates the drift and increases the coverage of the distribution (c). We used the EDM sampler (Karras et al., 2022) for this experiment.

Table 4: Compatibility of APG with CADS (Sadat et al., 2024a) and IG (Kynkäänniemi et al., 2024). Combining APG with other methods that improve diversity results in better FID than each method in isolation.

(a) CADS						(b) Interval guidance (IG)					
Guidance	FID ↓	Precision ↑	Recall ↑	Saturation ↓	Contrast ↓	Guidance	FID ↓	Precision ↑	Recall ↑	Saturation ↓	Contrast ↓
CFG	10.42	0.85	0.48	0.46	0.27	CFG	10.42	0.85	0.48	0.46	0.27
+CADS	8.65	0.85	0.56	0.43	0.26	+IG	7.49	0.84	0.60	0.39	0.25
+APG	6.49	0.85	0.62	0.33	0.21	+APG	6.49	0.85	0.62	0.33	0.21
+both	5.56	0.84	0.64	0.32	0.21	+both	5.29	0.84	0.65	0.33	0.22

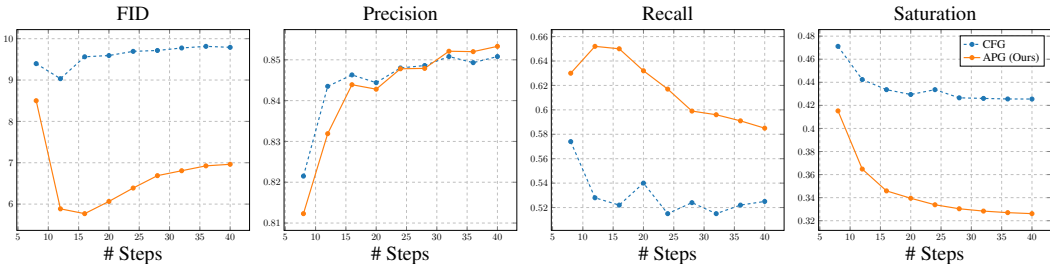


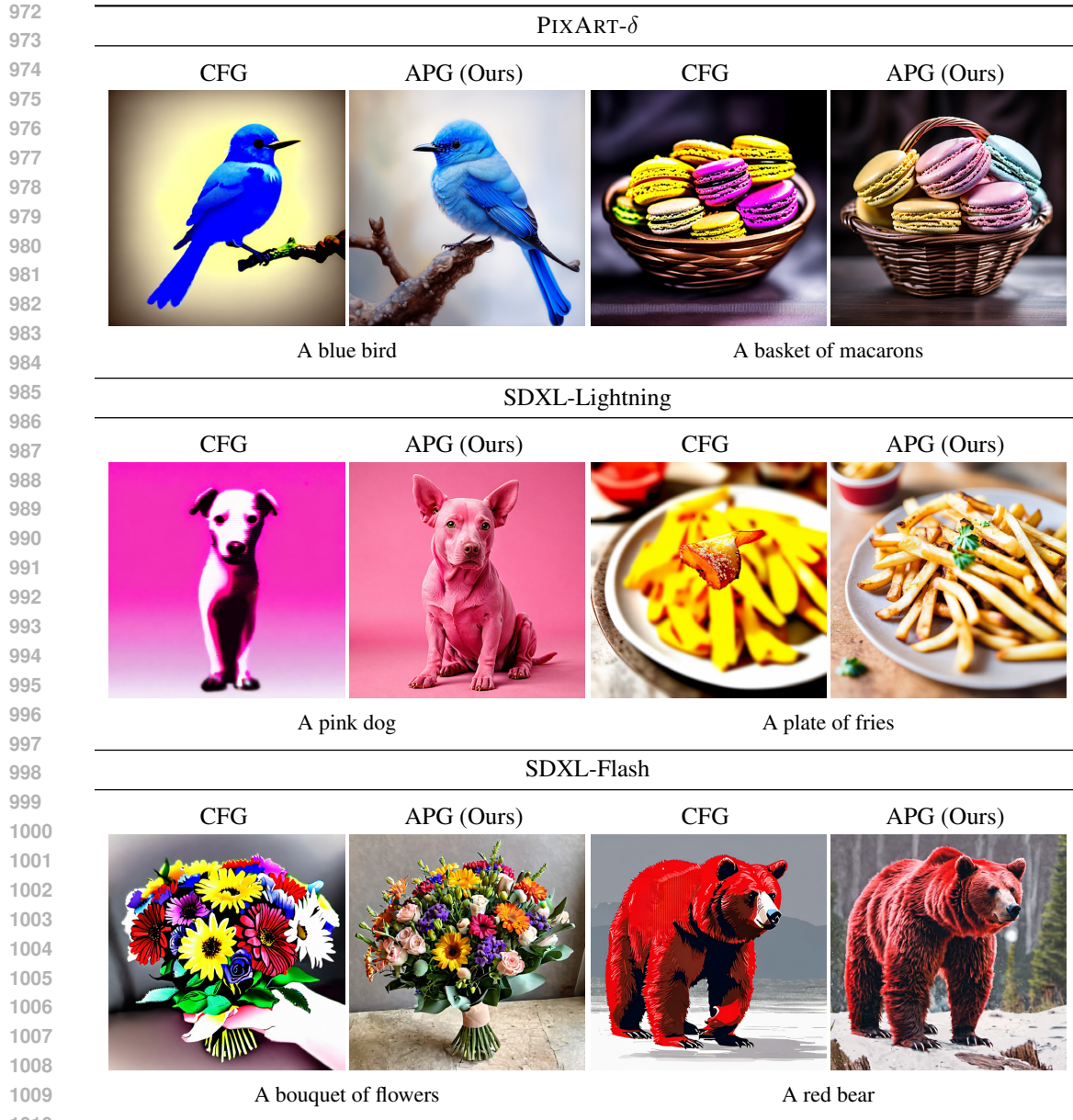
Figure 14: Comparison of CFG and APG across different numbers of sampling steps. APG consistently achieves better FID and recall while maintaining comparable or superior precision to CFG.

C.2 APG VS NUMBER OF SAMPLING STEPS

We now present the performance comparison between APG and CFG across different numbers of sampling steps using the EDM2 model. Figure 14 indicates that APG consistently provides better FID, recall, and saturation level while maintaining the same level of precision.

C.3 USING APG WITH DISTILLED MODELS

In this section, we show the compatibility of APG with distilled models using PIXART- δ (Chen et al., 2024), SDXL-Lightning (Lin et al., 2024c), and SDXL-Flash (sd community). Consistent with the main text, Figure 15 demonstrates that replacing CFG with APG significantly improves generation quality and saturation level across all models. This is also consistent with Figure 14, where APG outperforms CFG at fewer sampling steps (e.g., 8-16).



1011 Figure 15: Extended results showcasing the compatibility of APG with distilled diffusion models.
1012 Compared to CFG, using APG does not lead to degradation in the output quality.
1013

1014 C.4 COMPATIBILITY WITH DIFFERENT SAMPLERS

1015 While the main experiment in Table 1 used the default sampler of each model, we next separately show
1016 that APG is compatible with different sampling algorithms widely used with diffusion models. As
1017 shown in Table 5, using APG with different samplers results in improved FID, recall, and saturation
1018 scores, consistent with the main findings in Table 1. We used class-conditional generation using
1019 DiT-XL/2 for this experiment.
1020
1021

1022 C.5 COMPATIBILITY WITH ICG

1023 Independent condition guidance (ICG) (Sadat et al., 2024b) is a method to apply CFG without the
1024 need to query an unconditional model. In Table 6, we show that APG is compatible with ICG, and
1025

Table 5: Impact of using APG with popular diffusion samplers using the class-conditional ImageNet model (DiT-XL/2). Compared to CFG, APG shows improved metrics across all samplers.

Sampler	APG (Ours)			CFG		
	FID ↓	Recall ↓	Saturation ↓	FID ↓	Recall ↓	Saturation ↓
DDIM (Song et al., 2021a)	6.69	0.62	0.30	17.45	0.38	0.42
DPM++ (Lu et al., 2022b)	6.87	0.62	0.32	17.65	0.38	0.43
SDE-DPM++ (Lu et al., 2022b)	8.53	0.57	0.32	19.01	0.36	0.43
PNDM (Liu et al., 2022a)	5.37	0.68	0.32	16.50	0.40	0.43
UniPC (Zhao et al., 2023)	6.91	0.62	0.32	17.65	0.38	0.43

Table 6: Compatibility of APG and ICG. Combining APG with ICG significantly improves FID, recall, and saturation scores while maintaining similar precision.

Guidance	FID ↓	Precision ↑	Recall ↑	Saturation ↓	Contrast ↓
ICG	17.63	0.85	0.32	0.49	0.28
+APG (Ours)	5.73	0.85	0.63	0.33	0.22

Table 7: Compatibility of APG and TSG with. Combining APG with TSG improves FID, recall, and saturation scores while maintaining similar precision.

Guidance	FID ↓	Precision ↑	Recall ↑	Saturation ↓	Contrast ↓
TSG	14.00	0.81	0.52	0.37	0.28
+APG (Ours)	5.84	0.81	0.66	0.30	0.20

similar to CFG, using APG with ICG results in improved FID, recall, and saturation scores while maintaining similar precision. We use class-conditional ImageNet generation with EDM2-S for this experiment.

C.6 COMPATIBILITY WITH TSG

Time-step guidance (TSG) (Sadat et al., 2024b) is an extension of CFG that leverages the time-step information learned by the diffusion model to enhance the quality of generations. We next demonstrate that applying the update rule in APG further improves the performance of TSG. Table 7 shows that APG improves FID, recall, and saturation metrics, while maintaining similar precision to TSG. This experiment is based on class-conditional ImageNet generation using DiT-XL/2.

C.7 ALIGNMENT WITH THE CONDITION

We next demonstrate that replacing CFG with APG does not compromise the alignment between the input condition and the output. To validate this, we measure the classification accuracy of the generated results for the ImageNet task and the CLIP score for Stable Diffusion. The results in Table 8 show that both CFG and APG achieve comparable alignment metrics. Thus, APG reduces saturation and improves FID without compromising condition alignment.

Table 8: Condition alignment comparison between CFG and APG.

Alignment metric	CFG	APG
Class Accuracy ↑	0.97	0.96
CLIP-Score ↑	0.31	0.31

C.8 EXTENDED ABLATION STUDIES

Effect of the parallel component We next demonstrate the effect of η on the generated images in Table 9a. As hypothesized in Section 4, increasing the strength of the parallel component leads to higher saturation levels and increased FID. We recommend setting $\eta = 0$ by default and only increasing it if more saturation is desired in the generated images.

Table 9: Ablation study examining various design elements in APG.

(a) Influence of η			(b) Impact of rescaling r			(c) Effect of momentum β		
η	FID \downarrow	Saturation \downarrow	r	FID \downarrow	Recall \uparrow	β	FID \downarrow	Recall \uparrow
0.0	6.49	0.33	0.25	7.45	0.72	-1.5	13.38	0.73
0.25	6.49	0.34	2.5	6.49	0.62	-0.75	6.49	0.62
0.5	6.49	0.36	10	7.97	0.57	0.0	6.84	0.60
1.0	6.63	0.37	∞	7.93	0.56	0.5	7.10	0.59

Table 10: Hyperparameters used in the main experiment (Table 1).

Model	w	η	r	β
EDM2-S	4	0	2.5	-0.75
EDM2-XL	2	0	2.5	-0.75
DiT-XL/2	4	0	5	-0.50
Stable Diffusion 2.1	10	0	7.5	-0.75
Stable Diffusion XL	15	0	15	-0.50

Effect of the rescaling threshold The effect of the rescaling radius r on the generated images is shown in Table 9b. Excessive rescaling degrades image quality, while high values of r result in no noticeable change, as the rescaling function approaches the identity function. Therefore, midrange values for r yield better FID scores. We suggest observing the norm of ΔD_t during the inference process and choosing r in a way that is comparable (on average) to the norm of ΔD_t .

Effect of the momentum strength Table 9c shows the effect of momentum strength β on generation quality. Note Negative values for β result in better FID compared to positive momentum, and excessive momentum degrades image quality. This aligns with our hypothesis that moving away from the previous directions helps limit the drift that can occur during sampling with higher guidance scales. Empirically, we found that $\beta \in [-0.75, -0.25]$ works well in most setups.

D IMPLEMENTATION DETAILS

We provide the code for APG in Algorithm 1. Compared to CFG, APG only includes a few additional lines of code without noticeable computational overhead. As discussed in Section 4, we always convert the predictions of the diffusion model to $D_\theta(z_t, t, \mathbf{y})$, compute the guided prediction, and convert it back to the initial output type at each sampling step.

We mainly use the ADM evaluation suite (Dhariwal & Nichol, 2021) for computing FID, precision, and recall. The FID is computed using 10,000 generated images and the whole training set for class-conditional ImageNet models. For text-to-image models, the FID is evaluated using the evaluation subset of MS COCO 2017 (Lin et al., 2014). The hyperparameters used for the main experiment are given in Table 10.

E MORE VISUAL RESULTS

This section presents extended visual comparisons between APG and CFG. Additional results using EDM2 are provided in Figure 16, with an example of how APG enhances diversity shown in Figure 17. Further images for Stable Diffusion 2.1 and Stable Diffusion XL are included in Figures 18 and 19. Moreover, Figure 20 illustrates how APG improves text spelling in Stable Diffusion 3. Finally, more examples of APG applied to distilled models are shown in Figures 21 to 23.

1134
1135
1136
1137
1138
1139
1140
1141
1142
1143
1144
1145
1146
1147
1148
1149
1150
1151
1152
1153
1154
1155
1156
1157
1158
1159
1160
1161
1162
1163
1164
1165
1166
1167
1168
1169
1170
1171
1172
1173
1174
1175
1176
1177
1178
1179
1180
1181
1182
1183
1184
1185
1186
1187

Algorithm 1 PyTorch implementation of APG.

```

import torch

class MomentumBuffer:
    def __init__(self, momentum: float):
        self.momentum = momentum
        self.running_average = 0

    def update(self, update_value: torch.Tensor):
        new_average = self.momentum * self.running_average
        self.running_average = update_value + new_average

def project(
    v0: torch.Tensor, # [B, C, H, W]
    v1: torch.Tensor, # [B, C, H, W]
):
    dtype = v0.dtype
    v0, v1 = v0.double(), v1.double()
    v1 = torch.nn.functional.normalize(v1, dim=[-1, -2, -3])
    v0_parallel = (v0 * v1).sum(dim=[-1, -2, -3], keepdim=True) * v1
    v0_orthogonal = v0 - v0_parallel
    return v0_parallel.to(dtype), v0_orthogonal.to(dtype)

def normalized_guidance(
    pred_cond: torch.Tensor, # [B, C, H, W]
    pred_uncond: torch.Tensor, # [B, C, H, W]
    guidance_scale: float,
    momentum_buffer: MomentumBuffer = None,
    eta: float = 1.0,
    norm_threshold: float = 0.0,
):
    diff = pred_cond - pred_uncond
    if momentum_buffer is not None:
        momentum_buffer.update(diff)
        diff = momentum_buffer.running_average
    if norm_threshold > 0:
        ones = torch.ones_like(diff)
        diff_norm = diff.norm(p=2, dim=[-1, -2, -3], keepdim=True)
        scale_factor = torch.minimum(ones, norm_threshold / diff_norm)
        diff = diff * scale_factor
    diff_parallel, diff_orthogonal = project(diff, pred_cond)
    normalized_update = diff_orthogonal + eta * diff_parallel
    pred_guided = pred_cond + (guidance_scale - 1) * normalized_update
    return pred_guided

```

1188
1189
1190
1191
1192
1193
1194
1195
1196
1197
1198
1199
1200
1201
1202
1203
1204
1205
1206
1207
1208
1209
1210
1211
1212
1213
1214
1215
1216
1217
1218
1219
1220
1221
1222
1223
1224
1225
1226
1227
1228
1229
1230
1231
1232
1233
1234
1235
1236
1237
1238
1239
1240
1241



Figure 16: More visual results comparing APG and CFG using EDM2.

1242
1243
1244
1245
1246
1247
1248
1249
1250
1251
1252
1253
1254
1255
1256
1257
1258
1259
1260
1261
1262
1263
1264
1265
1266
1267
1268
1269
1270
1271
1272
1273
1274
1275
1276
1277
1278
1279
1280
1281
1282
1283
1284
1285
1286
1287
1288
1289
1290
1291
1292
1293
1294
1295

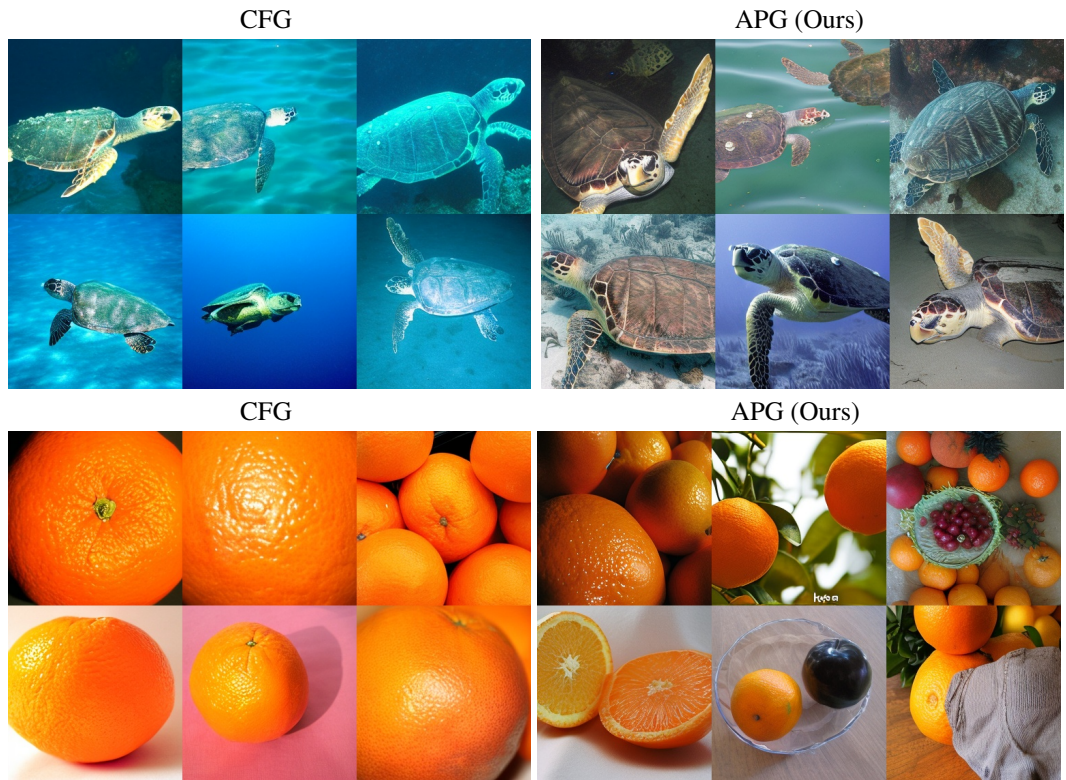


Figure 17: Showcasing the diversity of generations after using APG. APG removes oversaturation issues while improving diversity w.r.t. the overall image composition.

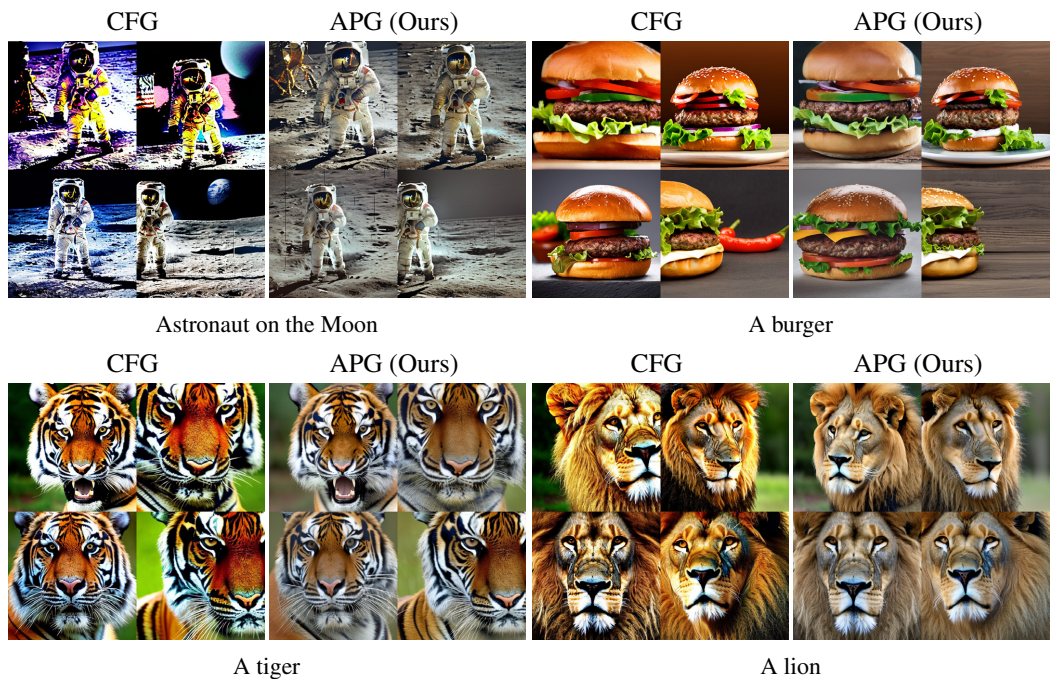


Figure 18: More visual examples comparing CFG and APG using Stable Diffusion 2.1.

1296
1297
1298
1299
1300
1301
1302
1303
1304
1305
1306
1307
1308
1309
1310
1311
1312
1313
1314
1315
1316
1317
1318
1319
1320
1321
1322
1323
1324
1325
1326
1327
1328
1329
1330
1331
1332
1333
1334
1335
1336
1337
1338
1339
1340
1341
1342
1343
1344
1345
1346
1347
1348
1349

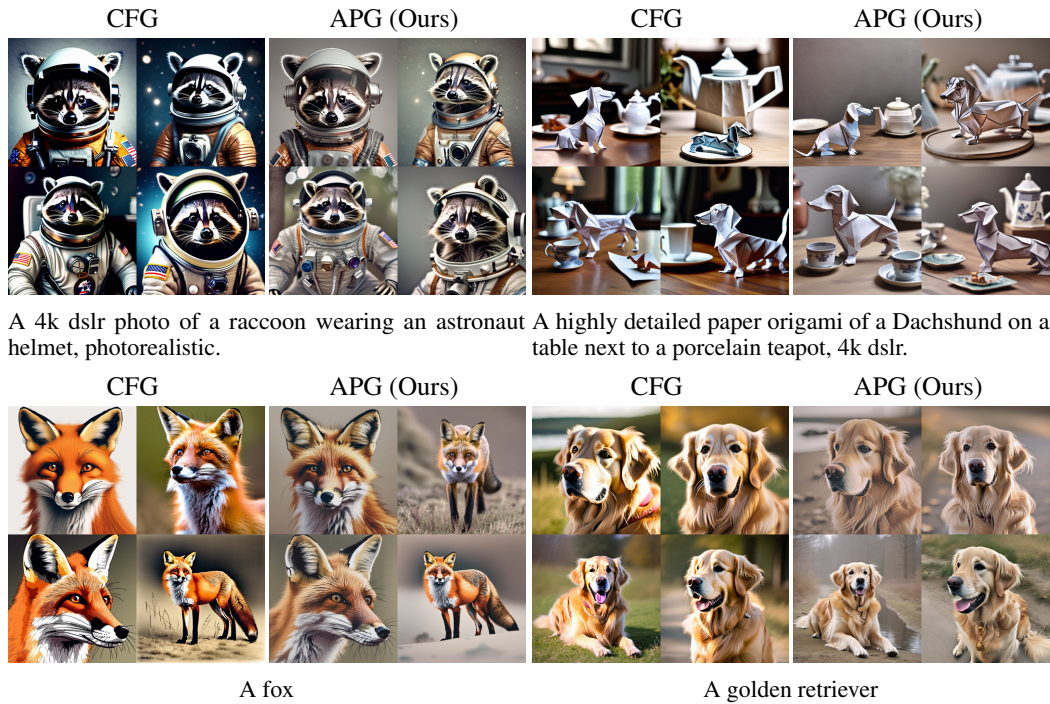


Figure 19: More visual examples comparing CFG and APG using Stable Diffusion XL.

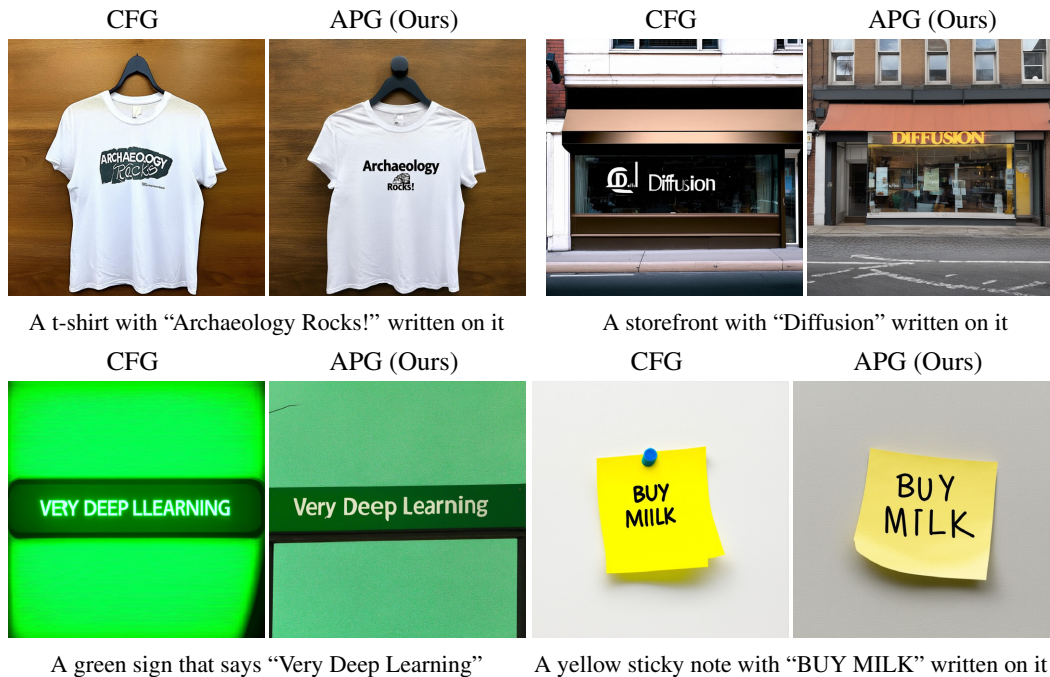


Figure 20: Additional visual examples on the quality of rendering text using Stable Diffusion 3. Compared to CFG, APG results show more consistent spellings.

1350
 1351
 1352
 1353
 1354
 1355
 1356
 1357
 1358
 1359
 1360
 1361
 1362
 1363
 1364
 1365
 1366
 1367
 1368
 1369
 1370
 1371
 1372
 1373
 1374
 1375
 1376
 1377
 1378
 1379
 1380
 1381
 1382
 1383
 1384
 1385
 1386
 1387
 1388
 1389
 1390
 1391
 1392
 1393
 1394
 1395
 1396
 1397
 1398
 1399
 1400
 1401
 1402
 1403

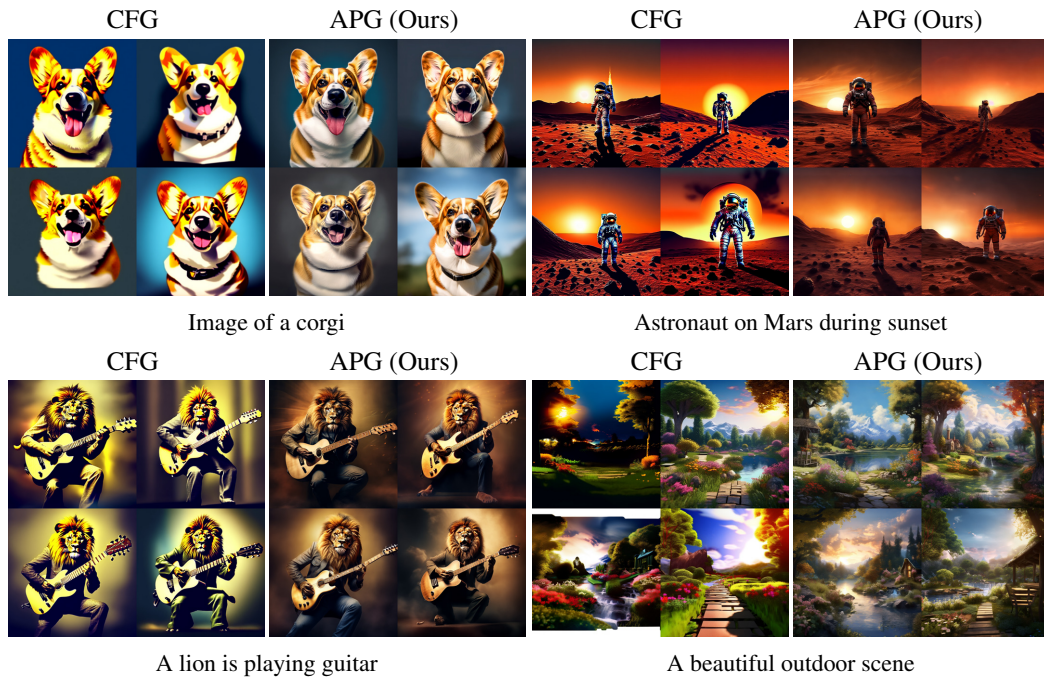


Figure 21: More visual examples comparing CFG and APG using PIXART- δ .

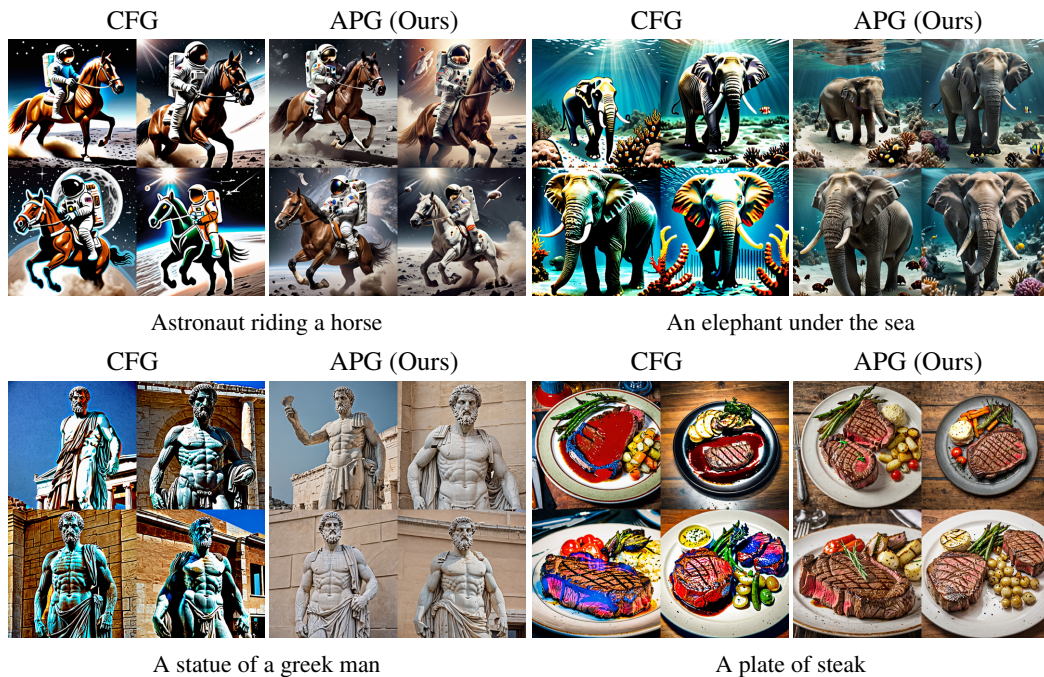


Figure 22: More visual examples comparing CFG and APG using SDXL-Flash.

1404
1405
1406
1407
1408
1409
1410
1411
1412
1413
1414
1415
1416
1417
1418
1419
1420
1421
1422
1423
1424
1425
1426
1427
1428
1429
1430
1431
1432
1433
1434
1435
1436
1437
1438
1439
1440
1441
1442
1443
1444
1445
1446
1447
1448
1449
1450
1451
1452
1453
1454
1455
1456
1457

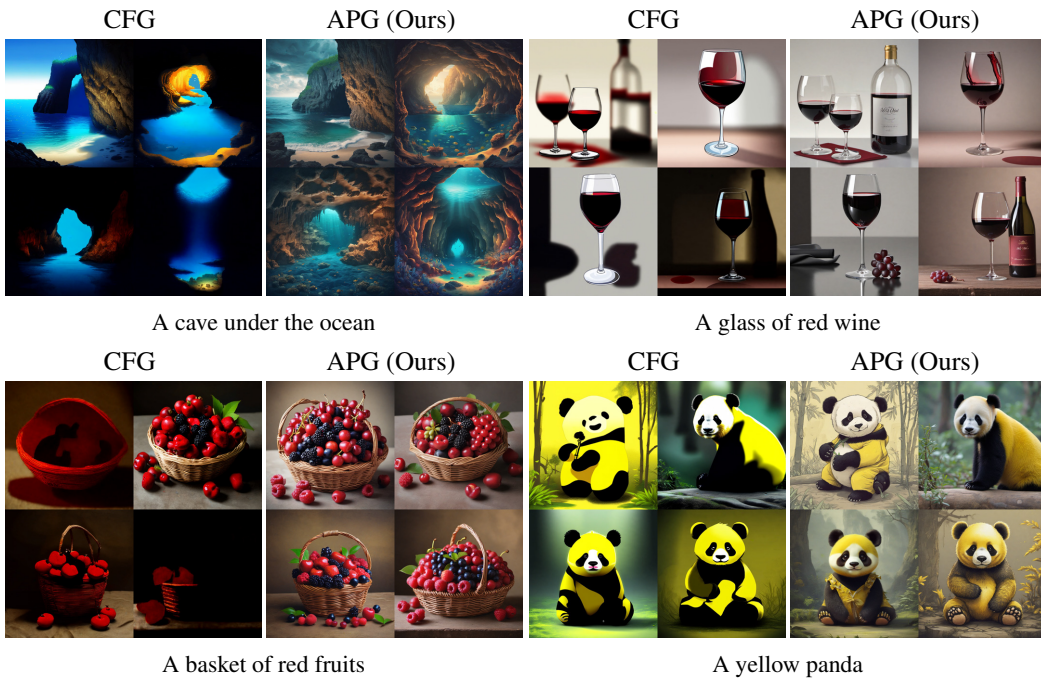


Figure 23: More visual examples comparing CFG and APG using SDXL-Lightning.